Check for updates

ADVANCED MATERIALS
www.advmat.de

Artificial Neuronal Devices Based on Emerging Materials: Neuronal Dynamics and Applications

Hefei Liu, Yuan Qin, Hung-Yu Chen, Jiangbin Wu, Jiahui Ma, Zhonghao Du, Nan Wang, Jingyi Zou, Sen Lin, Xu Zhang, Yuhao Zhang,* and Han Wang**

Artificial neuronal devices are critical building blocks of neuromorphic computing systems and currently the subject of intense research motivated by application needs from new computing technology and more realistic brain emulation. Researchers have proposed a range of device concepts that can mimic neuronal dynamics and functions. Although the switching physics and device structures of these artificial neurons are largely different, their behaviors can be described by several neuron models in a more unified manner. In this paper, the reports of artificial neuronal devices based on emerging volatile switching materials are reviewed from the perspective of the demonstrated neuron models, with a focus on the neuronal functions implemented in these devices and the exploitation of these functions for computational and sensing applications. Furthermore, the neuroscience inspirations and engineering methods to enrich the neuronal dynamics that remain to be implemented in artificial neuronal devices and networks toward realizing the full functionalities of biological neurons are discussed.

1. Introduction

Neuromorphic computing (NC) is a promising computational framework for overcoming the processing speed and power efficiency bottlenecks of the classical von Neumann computing architecture in learning, recognition, optimization, and classification applications. In terms of hardware, the key concept is to build a computing system that physically emulates the structure and working mechanism of mammalian brains. The fundamental building blocks for such systems are artificial synaptic and neuronal devices with sufficient biologically plausible dynamics so that the physical processes associated with perception and learning can be reasonably replicated in artificial neural network (ANN) hardware. In such bio-inspired neural networks, neurons play the role of information integrator and processor. Synapses, which are the connection between neurons, transmit and store the processed information. Early NC systems are mainly based on conventional complementary metal-oxide-semiconductor (CMOS) technology, such as the IBM TrueNorth chip, the Loihi chip by Intel, and the Tensor Processing Unit developed by Google.[1] However, CMOS-based artificial neurons typically take tens of transistors to form a single spiking neuron with limited neuronal dynamics, which makes CMOS neuromorphic chips far from ideal in terms of scalability and energy efficiency.[2] Therefore, a number of emerging volatile switching materials and technologies beyond silicon CMOS were introduced to building more compact, efficient, and biologically plausible artificial synapses and neurons.[3] Nonvolatile memory devices such as resistive RAM (memristor),[4] phase change memory (PCM),[5] and spin-transfer torque RAM have been widely demonstrated as synaptic components in a neural network.[6] Arrays of these devices can implement the memory (storage and update of synaptic weight) and computing (e.g., dot-product machine) functions of synapses, many types of synaptic plasticity, and have demonstrated a diversity of computing tasks ranging from multilayer perception networks, differential equation solvers, to convolutional neural networks for image recognition, etc.[7] In these demonstrations, synapse arrays typically serve as in-memory computing units and vector-matrix-multiplication accelerators. The realization of the neuronal functions, such as signal accumulation and activation

H. Liu, H.-Y. Chen, J. Wu, J. Ma, Z. Du, H. Wang
Ming Hsieh Department of Electrical and Computer Engineering
University of Southern California
Los Angeles, CA 90089, USA
E-mail: han.wang.4@usc.edu

Y. Qin, Y. Zhang
Center for Power Electronics Systems
Bradley Department of Electrical and Computer Engineering
Virginia Polytechnic Institute and State University
Blacksburg, VA 24060, USA
E-mail: yhzhang@vt.edu

N. Wang, H. Wang
Mork Family Department of Chemical Engineering and Materials Science
University of Southern California
Los Angeles, CA 90089, USA

J. Zou, S. Lin, X. Zhang
Department of Electrical and Computer Engineering
Carnegie Mellon University
Pittsburgh, PA 15213, USA
E-mail: xuzh@cmu.edu

The ORCID identification number(s) for the author(s) of this article can be found under https://doi.org/10.1002/adma.202205047.

© 2023 The Authors. Advanced Materials published by Wiley-VCH GmbH. This is an open access article under the terms of the Creative Commons Attribution-NonCommercial-NoDerivs License, which permits use and distribution in any medium, provided the original work is properly cited, the use is non-commercial and no modifications or adaptations are made.

DOI: 10.1002/adma.202205047

function, largely relied on software or digital circuits. However, CMOS-based neurons suffer from scalability issue, limited neuronal dynamics, and unsatisfactory energy consumption compared with biological nervous systems. The computing resource and power budget required by software-based neurons are even higher. To realize more practical application of advanced computing architectures such as coupled oscillatory neural networks (ONNs) and spiking neural networks (SNNs), it is essential to incorporate artificial neuronal devices with spatial-temporal integration, probabilistic activation function, neuronal coupling, and hopefully more sophisticated neuronal dynamics to appropriately regulate the information processing in NC hardware.

A variety of devices based on emerging materials with volatile threshold switching properties have been reported in the literature to demonstrate neuronal features, including insulator-metal-transition (IMT) oscillators,[8] valence change mechanism (VCM) and electrochemical metallization (ECM) memristors,[9] PCM,[10] magnetic tunnel junctions (MTJs),[11] magnetic skyrmion devices,[12] ferroelectric field effect transistors (FeFETs),[13] and superconducting nanowire oscillators.[14] To be clear, the artificial neurons or artificial neuronal devices in this paper, except specially stated, refer to the devices which employ volatile switching materials as the core functional part, instead of those based on digital computers or CMOS technology. Despite distinct switching physics and operation mechanisms,[15] their neuronal behaviors can be described by a few neuron models, namely, the oscillatory neurons, leaky integrate-and-fire (LIF) neurons, and Hodgkin–Huxley (HH) neurons.[16] Some of the demonstrated artificial neurons also exhibit stochastic properties.[10a,17] **Figure 1** summarizes the research areas of interest on artificial neurons, including the implemented neuron models, sensory neurons, architectures of neural networks, and their applications.[18]

In this paper, we review the physically demonstrated artificial neuronal devices based on volatile switching materials from the angle of implemented neuron models, neuronal dynamics, and their applications in both computation and sensing. At the individual device level, various switching mechanisms to implement a certain type of neuron are briefly introduced and compared. The performance of the state-of-the-art neuronal oscillators and LIF neurons are benchmarked. At the system level, we discuss which aspects of neuronal dynamics are captured by each type of neuronal devices and how the corresponding ANN hardware is enabled for fulfilling computational tasks. Besides, efforts of integrating these neuronal devices with sensors to form various sensory neurons are also summarized. Furthermore, we share our perspective on how to bridge the gap between artificial and biological neurons toward developing more advanced neural network applications.

This review article is structured as follows: Section 2 introduces the biological inspirations of artificial neuronal devices and provides a summary of previous reports on this topic. Each of three demonstrated neuron models takes a subsection. Section 2.1 introduces and compares various switching mechanisms for implementing neuronal oscillators, including IMT, VCM, MTJ, and FeFET. Typical dynamics of neuronal oscillators, including frequency coding, stochastic activation, and coupling capability, as well as the enabled computing architectures, such as Boltzmann machine (BM) and ONN, are also reviewed. Section 2.2 summarizes the approaches to building LIF neurons, including both capacitor-based circuits and capacitor-free scenarios. The dynamics of LIF neuron, including spatial-temporal integration, probabilistic firing,

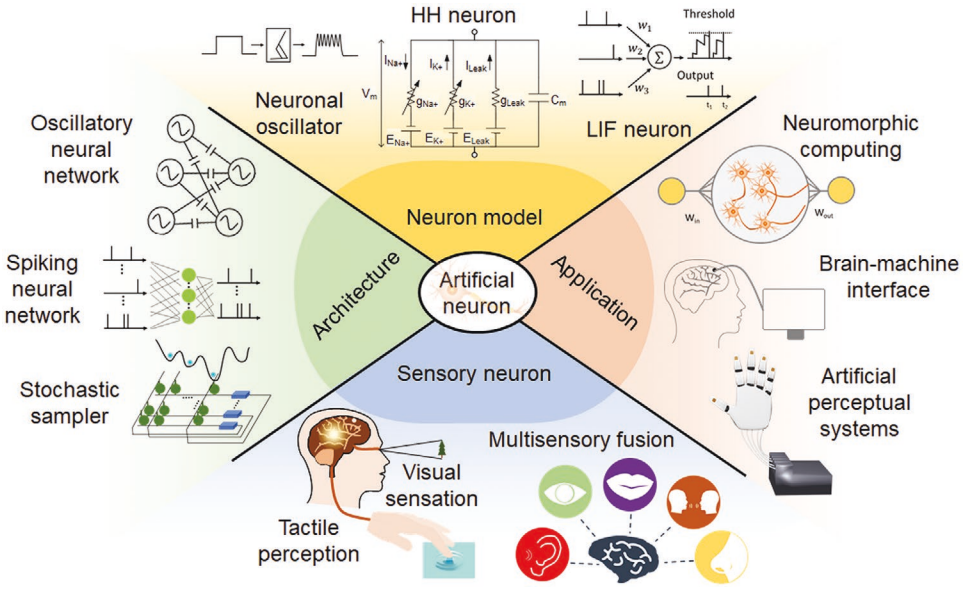

Figure 1. Summary of the research on artificial neurons, including the implemented neuron models, sensory neurons, architectures of neural networks, and their applications. The three main implemented neuron models are neuronal oscillator, leaky integrate-and-fire (LIF) neuron, and Hodgkin–Huxley (HH) neuron. Several types of neural networks can be constructed based on the features of these neuron models, such as oscillatory neural networks, spiking neural networks, and stochastic samplers. Combining artificial neuronal devices with sensors forms various sensory neurons with the function of visual sensation, tactile perception, and multisensory fusion. The development of artificial neurons enables a series of applications ranging from NC, brain-machine interface, to artificial perceptual systems.

© 2023 The Authors. Advanced Materials published by Wiley-VCH GmbH

15214095, 0, Downloaded from https://onlinelibrary.wiley.com/doi/10.1002/adma.202205047, Wiley Online Library on [19/06/2023]. See the Terms and Conditions (https://onlinelibrary.wiley.com/terms-and-conditions) on Wiley Online Library for rules of use; OA articles are governed by the applicable Creative Commons License

along with frequency adaption and neuronal inhibition are discussed. The applications of these neuronal dynamics in SNNs and probabilistic computing paradigms, such as probabilistic population coding (PPC) and Bayesian networks (BNs), are reviewed. Section 2.3 introduces the research progress of demonstrating HH neurons with high-order neuronal dynamics, and briefly discusses its potential toward more energy-efficient neural networks. Section 3 reviews the research efforts of combining neuronal devices with various sensors to form sensory neurons. Their applications in visual sensation, tactile perception, and multisensory fusion, as well as the attempts to realize sensation-storage-processing integrated perceptual systems are reviewed. Finally, Section 4 provides a perspective on three aspects of future research on artificial neurons: optimization of individual devices, improvement of demonstrated ANN architectures, and exploitation of more advanced neuronal dynamics in future neural networks.

2. Artificial Neurons for Computation

Compared to artificial synaptic devices, developing artificial neurons is a more challenging task owing to their structural and functional complexity. **Figure 2** illustrates the structure of a typical biological neuron which consists of several key functional parts: the soma, the axon, and the dendrites.[16,19] Synapses connect the axon of a (pre-synaptic) neuron to the dendrites (or soma) of another (post-synaptic) neuron. The information in biological nervous systems is encoded by neural spike trains, which are electrical impulse sequences propagating along the cell membrane of neurons. The neural spikes are generated by the axon hillock where the axon originates. The membrane potential (MP) of axon hillocks can be elevated by an arriving input neural spike. If the MP exceeds a certain threshold, the axon hillock fires a neural spike, passes it to the axon, and resets the MP to the resting status. Through this process, the axon hillock can integrate the inputs from the synapses and transform the input spike trains into an output signal, which would be sent to the next layer of neurons. The processing results are stored in synapse connection strength (synaptic weight) which are updated according to synaptic plasticities, such as spike rate-dependent plasticity and spike time-dependent plasticity (STDP).

Biological neurons have a few essential features which set requirements for their information processing capability. 1) The firing activity follows all-or-nothing law. If the MP does not reach the threshold, a neuron does not fire any spike, while when the stimulation intensity reaches the threshold, the neuron will fire a spike with the nearly fixed amplitude and duration. It has two consequences. First, information is encoded and processed by the frequency and pattern of neural spike trains, regardless of the width or specific shape of single spikes. Stronger stimulation should make a neuron fire more often and vice versa. Second, subthreshold MP does not cause a spiking event but spontaneously decays before being elevated by the next input spike, due to the ion diffusion through the

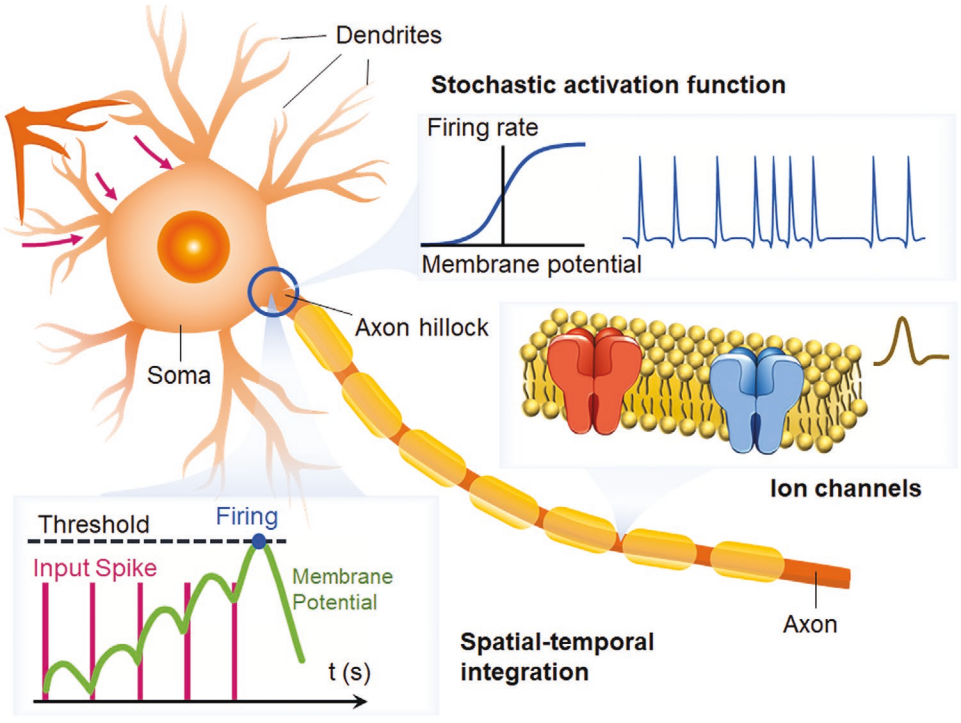

Figure 2. Schematics of a typical neuron. A typical neuron consists of the soma, the axon, and the dendrites. Some key neuronal features are highlighted, namely, the spatial-temporal integration of input spike trains, the short-term memory effect of membrane potential (the bottom left figure), the probabilistic sigmoidal activation function of axon hillock (the top right figure), and the ion channels on the cell membrane (the bottom right figure). These features enable neurons to collect information input from multiple synapses, analyze and encode the temporal correlation, process the information in a fault-tolerating manner, and generate output neural spike (action potential) trains following a set of rules.

© 2023 The Authors. Advanced Materials published by Wiley-VCH GmbH

15214095, 0, Downloaded from https://onlinelibrary.wiley.com/doi/10.1002/adma.202205047, Wiley Online Library on [19/06/2023]. See the Terms and Conditions (https://onlinelibrary.wiley.com/terms-and-conditions) on Wiley Online Library for rules of use; OA articles are governed by the applicable Creative Commons License

membrane. Because the arrival of input spikes has different time delay and strength attenuation depending on the traveling distance, the axon hillock therefore serves as a signal integrator with short-term memory, which enables the neuron to detect and create the spatial-temporal correlation in neural spike trains.[16] 2) The firing activity of neuron exhibits inherent stochasticity.[20] Neurophysiology research shows that the firing probability typically has a sigmoidal dependence on the MP so that the activation function of neural networks is naturally implemented by the probabilistic firing behavior of neurons.[21] The stochastic nature results in the random interspike interval in the spike train generated by a neuron excited by a constant stimulation level. As a result, biological nervous systems with intrinsic stochasticity tend to be more fault-tolerating as compared to deterministic digital computers.[22] 3) Biological neurons possess sophisticated membrane structures, especially the voltage-controlled ion channels that enable the energy-efficient regeneration and transport of action potentials, that is, neural spikes.[23] The complex membrane structure leads to high-order neuronal dynamics, such as refractory period (absolute and relative), variable firing mode, frequency adaption, and coherence resonance. They are related to the ultrahigh energy efficiency of individual biological neurons. At certain level of abstraction, the electrical characteristics of neuron membrane is described by the HH model.[16] 4) The interaction dynamics between multiple neurons and neuron groups also play a crucial role, such as coupling and synchronization, lateral inhibition and inhibitory neurons, and hierarchical control structures, which bring the complexity of biological nervous system to an overwhelmingly high level. Fortunately, the abovementioned features are not absolute requirements for implementing artificial neuronal devices and networks. Replicating a small fraction of them can already provide considerable computational power, and the selection of demonstrated neuronal dynamics depends on the specific computing framework and application goal, as we will show in the rest of the paper.

The signal accumulation and firing activity of neurons are typically abstracted as the weighted sum of inputs and activation function in ANNs implemented by traditional digital computers. By contrast, artificial neuronal devices based on volatile switching materials are a more faithful analog to biological neurons. As the resistive switching threshold acts as the MP threshold for triggering a neural spike and the volatile nature leads to a spontaneous relaxation process, these devices can generate oscillation waveforms or pulse trains which are comparable with neural spike trains. The neuronal dynamics realized by a type of neurons make them good candidates for implementing certain ANN architectures. For example, the coupling capability of neuronal oscillators leads to ONNs, and the spatial-temporal integration property of LIF neurons results in SNNs. On the other hand, the complexity of the switching physics provides the possibility of realizing more sophisticated neuronal dynamics represented by stochastic firing activity. Some probabilistic computing architectures, including BM, BN, and PPC, have been demonstrated. **Table 1** gives an overview of the ANNs demonstrated based on artificial neuronal devices. In the rest of this section, we will introduce the device mechanisms, discuss which aspects of neuronal dynamics are realized by each type of neuronal devices, and explain their roles in the ANN architectures.

2.1. Simple Artificial Neuronal Oscillators

The research of artificial neuronal devices starts from the simplest case, oscillators. Usually, neuronal oscillators can only realize the function of generating oscillation waveforms which are regarded as firing neural spike trains, without any other components like the integrator, short-term memory, and other sophisticated structures. A simple DC excitation (voltage or current) as the predetermined MP is applied to oscillatory neurons and converted into continuous oscillation.

2.1.1. Device Mechanisms

There are a large variety of physical/chemical/biological processes that may produce oscillation. Among them, IMT materials, volatile memristors, FeFETs, and MTJs have been intensively investigated as neuronal oscillators. IMT oscillators are based on the first-order phase transition (Mott or Peierls transition) driven by external voltages in IMT materials like NbO_2,[28] VO_2,[29] and 1T-TaS_2.[30] At room temperature, the IMT materials are in their high resistance state (HRS). When the applied electric field exceeds a certain threshold, an IMT transition occurs, and the materials switch to low resistance state

Table 1. Hardware implementation of ANNs enabled by artificial neuronal devices based on volatile switching materials.

Network architecture	Spiking neural network	Oscillatory neural network	Boltzmann machine	Bayesian network
Neuron type	LIF	Oscillator	Oscillator	LIF or oscillator
Featured neuronal dynamics	Spatial-temporal integration	Neuronal coupling	Tunable stochastic activation	Tunable stochastic activation
Learning type	Deterministic	Deterministic	Probabilistic	Probabilistic
Learning algorithm	Hebbian rules or backpropagation	Synchronization	Simulated annealing	Bayesian inference
Cooperation with synaptic devices	Yes	No	No	No
Demonstrated applications	Pattern classification (supervised or unsupervised)	Pattern recognition, image processing, combinatorial optimization	Combinatorial optimization	Genetic regulatory networks
Reference	[8c,24]	[25]	[26]	[27]

© 2023 The Authors. Advanced Materials published by Wiley-VCH GmbH

15214095, 0, Downloaded from https://onlinelibrary.wiley.com/doi/10.1002/adma.202205047, Wiley Online Library on [19/06/2023]. See the Terms and Conditions (https://onlinelibrary.wiley.com/terms-and-conditions) on Wiley Online Library for rules of use; OA articles are governed by the applicable Creative Commons License

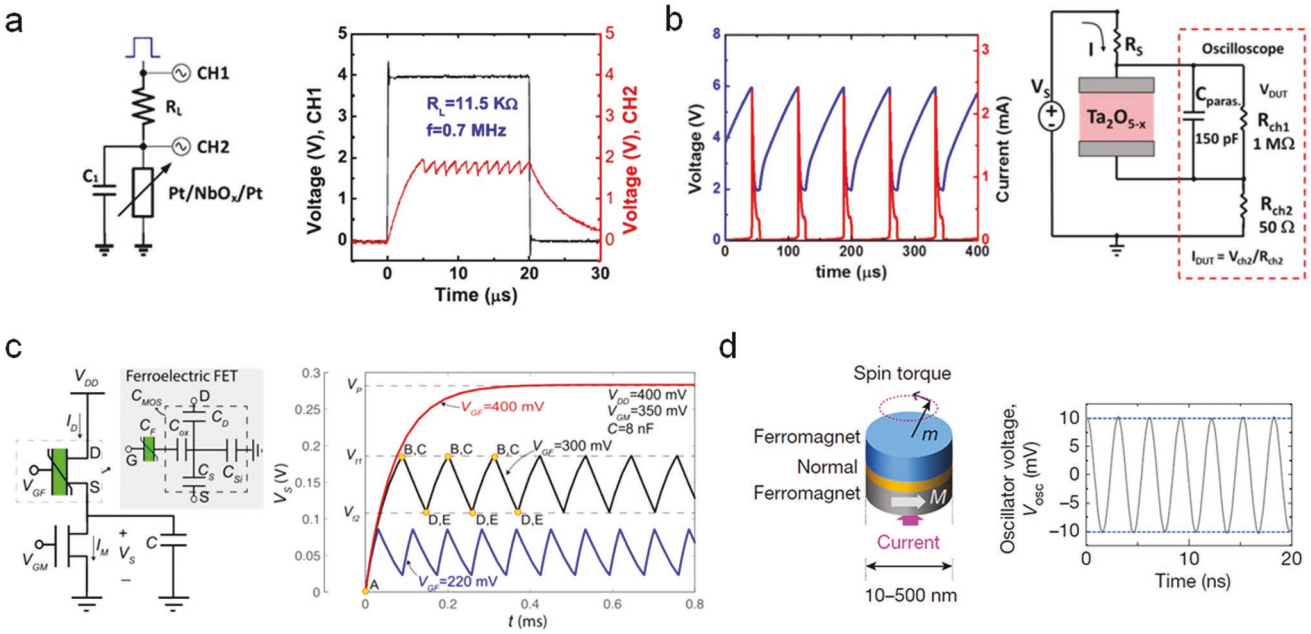

Figure 3. Typical oscillatory circuits and waveforms of various neuronal oscillators. a) IMT oscillator. Reproduced with permission.[8b] Copyright 2017, AIP Publishing. b) VCM memristor. Reproduced with permission.[9b] Copyright 2015, IEEE. c) FeFET-based oscillator. Reproduced with permission.[35] Copyright 2017, IEEE. d) MTJ oscillator. Reproduced with permission.[11d] Copyright 2017, Springer Nature.

(LRS). When the voltage is swept back, the reverse phase transition would occur at a lower threshold voltage. Therefore, a hysteresis window is formed, which plays a key role in generating oscillation. Connecting the IMT material to a series resistor and an optional parallel capacitor forms a Pearson–Anson oscillatory circuit (**Figure 3**a), which is a voltage divider. Careful design of the series resistance and the DC bias can make the load line of the resistor cross the hysteresis window. When the device is operated in this regime, the voltage across the IMT materials in HRS is over the higher threshold and the voltage across the LRS is below the lower threshold. As a result, neither the HRS nor the LRS is stable. The output voltage would go back and forth between the two threshold voltages and forms a continuous oscillation waveform. Volatile memristors, for example, TaO_x,[9b] HfO_2,[31] PCMO,[32] $Te/TiTe_2$,[33] and GeSe[34] memristors, share a similar hysteretic switching characteristic as IMT materials. Despite the switching physics is different, same design of oscillatory circuits also applies to these devices (Figure 3b). The only difference is that the switching behavior of volatile memristors does not involve crystal phase transition, but the formation-and-rupture of a temporary filament,[9b,33] transient Joule heating,[32b] or reversible ovonic threshold switching.[34]

FeFETs also have hysteresis switching features resulting from the polarization flip of ferroelectric materials.[35] In a typical ferroelectric oscillator circuit, the FeFET is connected to a MOSFET (the discharge FET) whose channel is in parallel with a capacitor (Figure 3c). Given the fixed drain voltage (V_{DD}) and gate voltage (V_{GF}) of the FeFET, increasing the source voltage (V_S) would decrease the gate-to-source voltage (V_{GS}) and induce the ferroelectric transition. The reverse transition would happen at a lower V_S (higher V_{GS}). Therefore, a hysteresis window forms in the I_{DS}–V_S curve, similar to the case of IMT oscillator. The oscillation can be induced by carefully tuning the DC bias voltages in the oscillatory circuit. If the load line of the discharge FET crosses the hysteresis window, a low V_S will trigger the ferroelectric flip, increase the conductivity of the FeFET, and pull up the V_S. Then, the elevated V_S induces the reverse ferroelectric flip, decrease the conductivity of the FeFET, and pull down the V_S. Such a cycle will be repeated and lead to the oscillation of the output V_S.[35] However, most reported FeFET-based artificial neurons are operated by pulse trains[13] instead of a DC source. Detailed investigation on the waveforms of FeFET oscillators remains very limited in the literature.

Different from the hysteretic switching devices, MTJs consist of a non-magnetic spacer sandwiched by two ferromagnetic layers (one free layer and one fixed layer).[6,17a,36] The magnetic multilayer structure converts the energy from a DC electrical current into oscillating output voltage through the periodic change of tunnel magnetoresistance via spin-transfer torque (Figure 3d). The electrical characteristics of neuronal oscillators based on different device concepts are greatly different. For comparison, the benchmarks of the reported neuronal oscillators are summarized in **Table 2**.

2.1.2. Neuronal Dynamics

The activation of neuronal oscillators typically follows a step function. The firing probability features an "all-or-nothing" manner defined by a threshold. Typical spike trains generated by neuronal oscillators are shown in Figure 3. Each oscillation peak is regarded as a neural spike. The refractory period, the time interval between two neural spikes, is almost constant as it is determined by the RC delay or the rotation speed of magnetic momentum. Such a continuous oscillation waveform in

© 2023 The Authors. Advanced Materials published by Wiley-VCH GmbH

15214095, 0, Downloaded from https://onlinelibrary.wiley.com/doi/10.1002/adma.202205047, Wiley Online Library on [19/06/2023]. See the Terms and Conditions (https://onlinelibrary.wiley.com/terms-and-conditions) on Wiley Online Library for rules of use; OA articles are governed by the applicable Creative Commons License

15214095, 0, Downloaded from https://onlinelibrary.wiley.com/doi/10.1002/adma.202205047, Wiley Online Library on [19/06/2023]. See the Terms and Conditions (https://onlinelibrary.wiley.com/terms-and-conditions) on Wiley Online Library for rules of use; OA articles are governed by the applicable Creative Commons License

Table 2. Benchmarks of the various neuronal oscillators.

Materials	Physics	Auxiliary circuit	Feature size F [μm][a)]	V_{in} [V]	Operating current [mA]	V_{osc}/V_{in}[b)]	Highest output frequency [MHz]	Ref.
NbO_2	IMT	1R1C[c)]	10	4	1	0.2/4 (5%)	≈2	[8b]
NbO_2	IMT	1R	0.3	2.5	0.015	1.4/2.5 (56%)	≈0.4	[37]
NbO_2	IMT	1R	5	1.65	0.5	1.2/1.65 (73%)	≈3.5	[38]
VO_2	IMT	1T1C[c)]	0.2	0.7	0.1	0.56/0.7 (80%)	≈0.05	[17b]
VO_2	IMT	1T1C	0.2	2	0.05	1.5/2 (75%)	≈0.12	[25b]
1T-TaS_2	IMT, charge density wave	1T1C	4	3.9	3	0.075/3.8 (2%)	≈2	[30]
1T-TaS_2	IMT, charge density wave	1R1C	0.6	2.2	1	0.05/2.2 (2.3%)	≈0.6	[39]
TaO_x	Filamentary	1R/1T	0.7	7	10	4/7 (57%)	≈250	[9b]
TaO_x	Filamentary	1R1C	2	6.8	2	1.5/6.8 (22%)	≈1	[40]
Te/$TiTe_2$/Pt	Filamentary	None	5	1.2	0.4	N/A	≈0.01	[33]
PCMO	Joule heating	1R1C	5	2.5	10	0.7/2.5 (28%)	≈0.18	[32b]
GeSe	Ovonic threshold switching	2R1C	4	5.4	3	2.7/4 (67.5%)	≈0.5	[34]
CoFe/Ru/CoFeB/MgO/CoFeB/CoFe	MTJ, spin-transfer torque	None	0.1	0.15	0.75	0.025/0.15 (17%)	>100 000	[36b]
FeB/MgO/CoFeB	MTJ, spin-transfer torque	None	0.375	0.25	6.5	0.02/0.25 (8%)	>10 000	[11d]

[a)]Feature area = $F \times F$ μm^2; [b)]V_{in}: the input voltage to the device, V_{osc}: the output oscillation voltage amplitude; [c)]R: resistor, T: transistor, C: capacitor.

which each neural spike is closely followed by another involves almost no memory effect. One important dynamic of neuronal oscillators is the frequency dependence on the MP. For the hysteretic switching devices, higher DC bias would facilitate the charge/discharge rate of the capacitor and enhance the firing rate.[8b] Zhang et al. demonstrated an afferent nerve based on a NbO_x oscillator and used the frequency dependence to capture the pressure evolution of touching.[37] For MTJs, larger applied DC currents also accelerate the spin-torque transfer and momentum rotation in the free layer, leading to higher firing frequency.[11d]

To implement more sophisticated neuronal dynamics, engineering efforts are made to bring nonlinear properties to these devices.[41] To enable the integration function, Cario et al. employed a group of more insulative Mott insulators to replace the common IMT materials in the oscillatory circuit.[42] The additional integration capability is attributed to the lower relaxation rate from the metastable low-resistivity state to the stable high-resistivity state. A more commonly used method for introducing LIF behaviors to hysteretic switching oscillators is adding a capacitor and a transistor (or a resistor) to the oscillatory circuit.[9c,43] The capacitor serves as an integrator while the accumulated charge can leak through the transistor or resistor. We will discuss the mechanisms and applications of LIF neurons later in Section 2.2.

More detailed investigations reveal the firing activity of memristive and IMT neurons possessing intrinsic stochasticity and chaotic dynamics.[17b,39,41,44] The stochasticity originates from the filament residue or the rearrangement of crystal domains.[17b,45] The threshold voltages of switching are not fixed but have cycle-to-cycle variations, as shown in **Figure 4**a. It has two consequences in the firing activity. First, if the load line of the resistor or transistor crosses the hysteresis window at boundaries (Figure 4a, $V_{GS} = 1.92$ V), the threshold variation will make whether the load line can cross the hysteresis window or not a random event. The output oscillation waveform is not continuous anymore but has random interspike intervals (Figure 4b), which corresponds to relative refractory periods. The dependence of firing probability on excitation voltage typically follows a sigmoidal probabilistic activation function (Figure 4c).[17b,39] Second, even if the load line crosses the central part of the hysteresis window, the amplitude of the continuous oscillation defined by two threshold voltages will still randomly change from cycle to cycle, which introduces stochastic features to the refractory.[39] Researchers proposed a stochastic sampling machine (SSM) neural network based on the probabilistic activation function, and demonstrated that stochastic neurons can enhance the handwritten digit recognition accuracy of an SSM network by up to 25% compared to deterministic neurons.[17b] Later, Yan et al. experimentally demonstrated simulated annealing using a BM based on six multiterminal stochastic memristive neuronal devices.[26a] The slope of the sigmoidal activation function can be tuned by applying an additional gate voltage, which can emulate a series of Fermi–Dirac distributions with different effective temperature parameters (Figure 4d,e). The researchers used the BM to solve a combinatorial optimization problem. The optimization result is represented by a Boolean vector. The system energy can be calculated given the current Boolean vector and the one with minimal energy represents the optimal solution. Over the optimization process, the value of each vector element is controlled by the firing activity of a stochastic neuron. In each iteration step, an excitation pulse was applied to a neuron. If the neuron fires, its corresponding Boolean value will be flipped, or otherwise remains the same. The stochastic neurons are sequentially updated until the system reaches the minimum energy. The performance of different temperature variation strategies is evaluated. The simulated annealing scenario, that is, changing

© 2023 The Authors. Advanced Materials published by Wiley-VCH GmbH

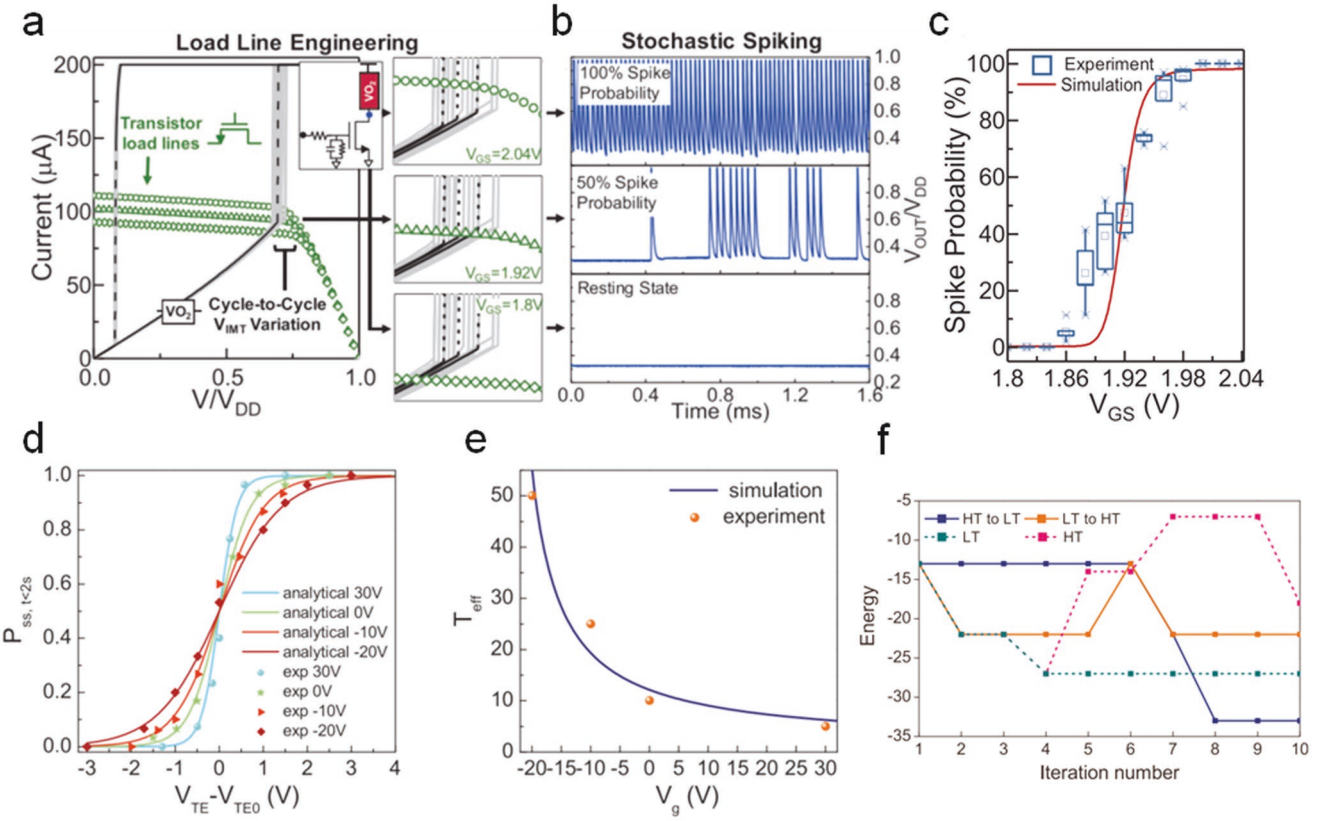

Figure 4. Stochastic properties of IMT and memristive neuronal oscillators. a) Stochastic spiking of a VO_2 oscillator operating in the stochastic oscillation regime where the transistor load lines cross the lower boundary of the hysteresis window. b) The stochastic oscillation waveforms, and c) the sigmoidal probabilistic activation curve. Reproduced with permission.[17b] Copyright 2017, IEEE. d) Gate tunable stochastic activation curves of a multi-terminal memristive neuron. e) The relation between the gate voltage and effective temperature of fitted Fermi–Dirac distributions. f) The energy evolution in the optimization process for different temperature variation strategies applied to the BM. Reproduced with permission.[26a] Copyright 2021, Springer Nature.

from high temperature to low temperature results in the most satisfactory energy evolution over the optimization process (Figure 4f).

MTJ devices with very small lateral dimensions are also reported to show stochasticity caused by thermal fluctuations, which can destabilize the magnetic configuration and generate stochastic oscillations between the parallel and anti-parallel states.[17a,46] MTJ devices have been proposed to build stochastic binary neurons for probabilistic computing frameworks such as PPC and BNs.[21c,27a,46,47] **Figure 5**a shows one of stochastic MTJ neuron circuits.[26b,48] The probability distribution for the MTJ to be in its parallel and anti-parallel states is controlled by the current passing through it, which is determined by the input voltage applied to the transistor gate terminal (V_{IN}). As a result, the probability distribution and the time average of V_{OUT} can be tuned by V_{IN} (Figure 5b). Such a dependence can be regarded as the probabilistic activation function, which is well fitted by a sigmoidal curve. The oscillation waveforms at different V_{IN} are shown in Figure 5c. Researchers interconnected eight stochastic MTJ neurons (also called probabilistic bits) through a microcontroller and a digital–analog converter (DAC) to form a BM (Figure 5c). As a demonstration, integer factorization problems are reformulated to be experimentally solved by the BM. The firing behavior of p stochastic neurons forms a binary vector, with firing and no-firing corresponding to 1 and 0, respectively. This vector represents an odd integer P no larger than 2^{p+1}. Other q neurons can represent another odd integer Q no larger than 2^{q+1}. P and Q are the two possible factors for a big integer no larger than 2^{p+q+2}. Owing to the probabilistic switching property of the neurons, the firing state of the two groups of neurons can represent all possible factor pairs of the big integer simultaneously, with a probability distribution depending on the synaptic inputs. Over the searching process, each neuron in the BM is driven by a synaptic input that is a function of all other neurons' outputs. Details about how to calculate the synaptic inputs for the next iteration are also explained in the paper.[26b] The BM can visit different states in the phase space with probabilities given by the Boltzmann law. Therefore, the solution with minimum energy would appear with highest probability. Some example results are shown in Figure 5e–g. Other spintronic device architectures, such as a nanomagnet with perpendicular magnetic anisotropy on top of a Hall bar, also exhibit stochastic properties which can be tuned by magnetic field induced by a current passing through a metal ring.[27a]

Besides probabilistic computing, stochasticity can also be exploited to extend the dynamics of neuronal devices. A couple of more advanced HH dynamics, as well as the

© 2023 The Authors. Advanced Materials published by Wiley-VCH GmbH

15214095, 0, Downloaded from https://onlinelibrary.wiley.com/doi/10.1002/adma.202205047, Wiley Online Library on [19/06/2023]. See the Terms and Conditions (https://onlinelibrary.wiley.com/terms-and-conditions) on Wiley Online Library for rules of use; OA articles are governed by the applicable Creative Commons License

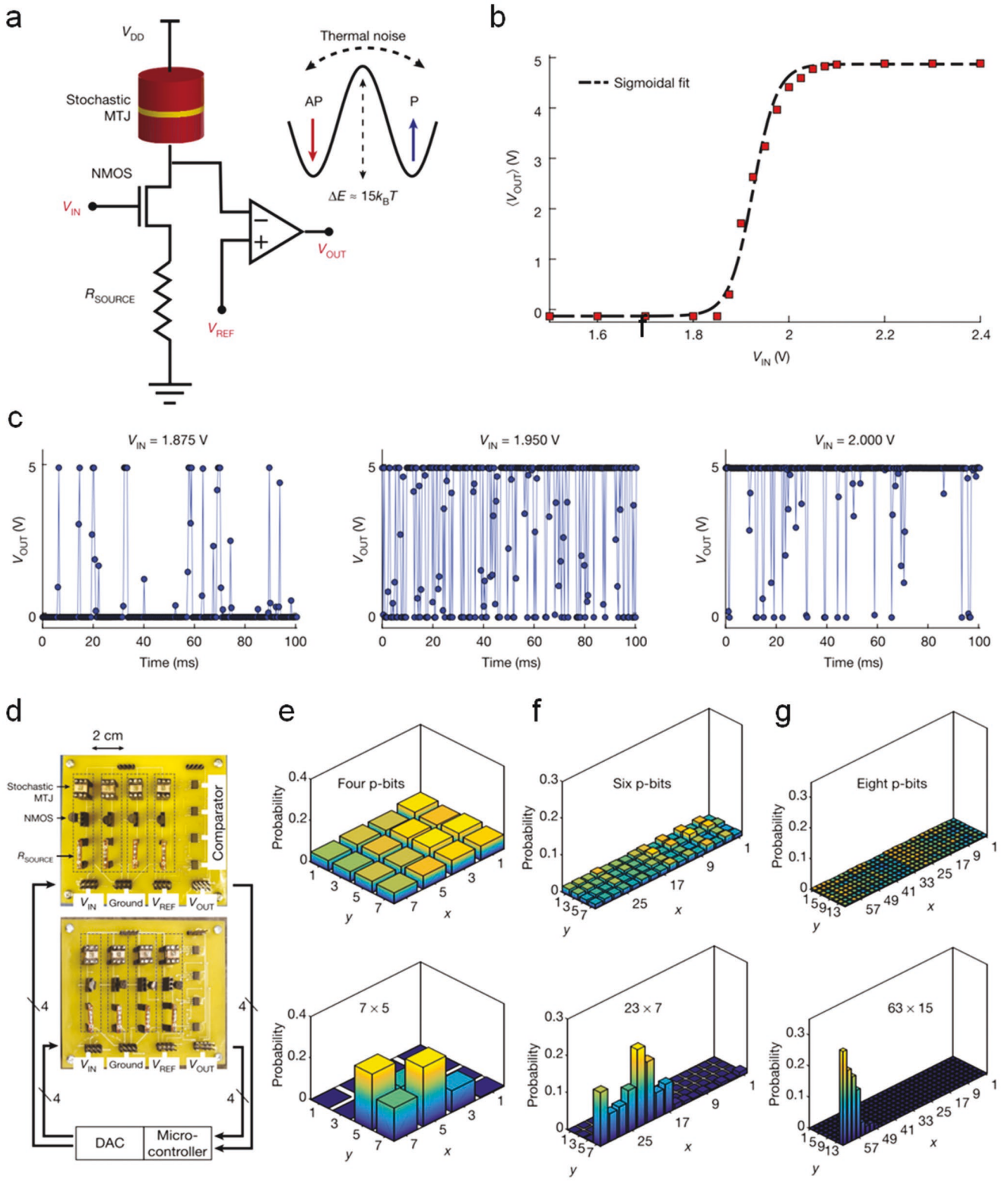

Figure 5. Stochastic properties of MTJ neurons for integration factorization. a) The circuit diagram of a stochastic MTJ neuron. b) Time-averaged V_{OUT}, as a function of the applied input (activation function), fitted to the sigmoidal function. c) Oscillation waveforms of V_{OUT} for three different V_{IN}, showing the different probability distribution of MTJ states. d) A photograph of a printed circuit board for eight stochastic MTJ neurons interconnected through a microcontroller and a DAC. e–g) The initial (top) and final (bottom) state of the system when four, six, and eight neurons are used to factorize $35 = 5 \times 7 = 7 \times 5$ (e), $161 = 23 \times 7$ (f), and $945 = 63 \times 15$ (g). Reproduced with permission.[26b] Copyright 2019, Springer Nature.

© 2023 The Authors. Advanced Materials published by Wiley-VCH GmbH

15214095, 0, Downloaded from https://onlinelibrary.wiley.com/doi/10.1002/adma.202205047, Wiley Online Library on [19/06/2023]. See the Terms and Conditions (https://onlinelibrary.wiley.com/terms-and-conditions) on Wiley Online Library for rules of use; OA articles are governed by the applicable Creative Commons License

frequency detection application, are implemented by a compact 1T-TaS_2 stochastic neuronal oscillator.[39] Stochastic properties are also expected to exist in FeFET oscillators, considering the similar hysteretic switching mechanism. Clues are captured by some reports;[13b,49] however, more solid evidence such as the detailed probabilistic activation curve and spike trains with random interspike intervals have not been experimentally investigated.

2.1.3. Oscillatory Neural Networks

Neuronal oscillators, even only with basic linear response properties, can be coupled with each other to form an ONN and execute data processing via the temporal correlation in the oscillating behaviors, more specifically, synchronization.[50] In ONNs, the information is encoded and processed by the phase and frequency in addition to the signal levels. Despite the fact that other types of artificial neuronal devices are also somewhat oscillatory, the phase and frequency of their spike trains are not well defined because they depend on the parameters of operating pulse trains. Here, we focus on the ONNs physically implemented using neuronal oscillators mentioned above. A comprehensive overview of coupled oscillator-based computing is presented in ref. [51].

In an ONN, the input to the network is encoded by a frequency or phase pattern. Driven by the input signal, the interconnected oscillators interact with each other and their oscillation behaviors reach synchronization, which is a stationary frequency or phase pattern that represents a minimum energy state.[52] The pattern can be extracted as the result of computation. Synchronization of interconnected neuronal oscillators has been experimentally demonstrated using TaO_x memristors,[9a,53] VO_2 oscillators,[54] and MTJs.[55] Coupling between FeFET oscillators is also proposed via simulation.[56] Two types of passive coupling, resistive (in-phase) and capacitive (antiphase), are realized (**Figure 6**a). Full interconnection between all oscillators can become overwhelming as the system size increases. To address this issue, some virtual connection strategies are proposed and physically realized. One solution is to employ a feedback mechanism to couple a single MTJ oscillator to the "time-delayed" copies of itself, like in reservoir computing.[11d,57] Another approach is to apply an external magnetic field to synchronize multiple MTJ oscillators (Figure 6b), or to couple many individual MTJ oscillators with an input microwave current (Figure 6c).[58]

Many computing applications have been demonstrated using ONNs. First, the degree of mutual synchronization between oscillators can act as a good measure of the Euclidean distance between two different input vectors.[59] Calculating Euclidean-distance of image patches and substituting the original pixel values with the distance values is equivalent to applying a Gabor filter to the image. This can be used for power efficient image processing.[56,60] Second, the neuronal oscillators can be synchronized with external signals whose frequency is close to the oscillators' intrinsic frequency. Single or multiple MJT neurons were employed to extract the frequency information of a preprocessed voice signal for spoken-digit and vowel recognition (Figure 6d), or to distinguish temporal sequences.[11d,55b,58] Third, the capacitive and resistive coupling between a few

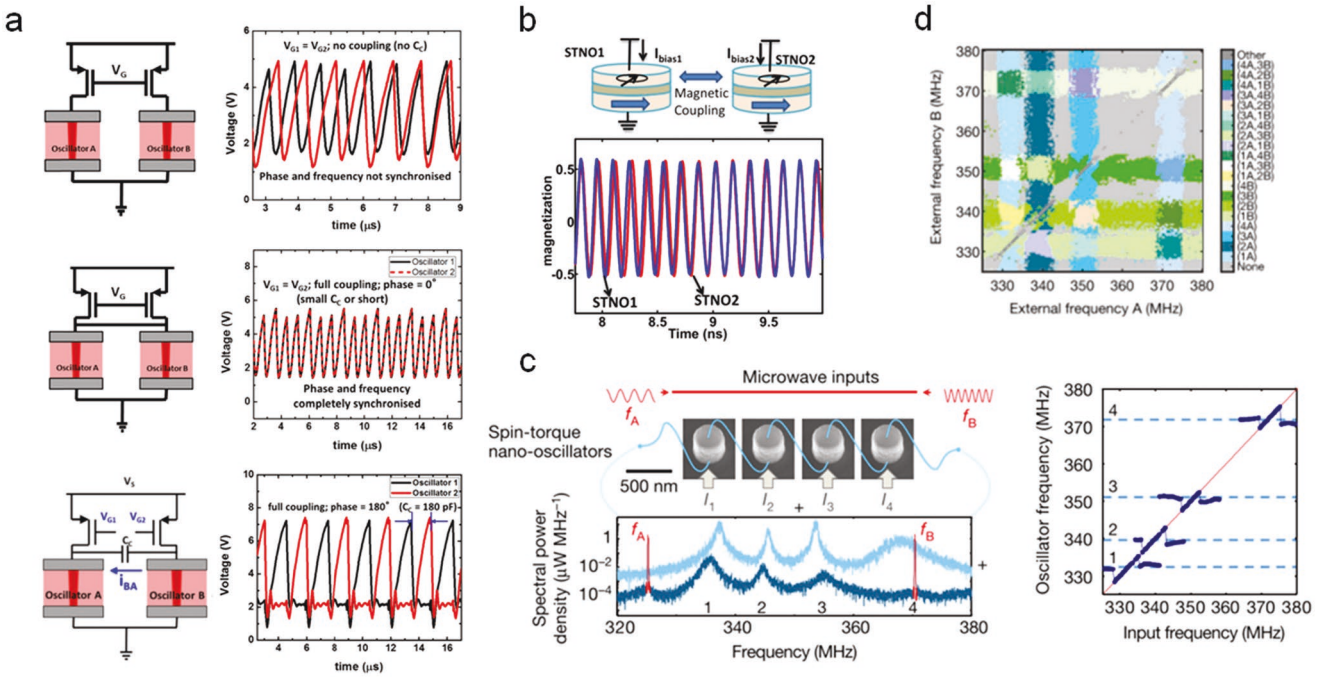

Figure 6. Different approaches to couple neuronal oscillators. a) From top to bottom: uncoupled, resistive (in-phase) coupled, and capacitive (antiphase) coupled VCM memristive oscillators. Reproduced with permission.[53b] Copyright 2015, IEEE. b) Synchronized MTJ oscillators via an external RF magnetic field. Reproduced with permission.[55a] Copyright 2015, IEEE. c) Synchronization between four MTJ oscillators and the input microwave signal and d) its application in vowel recognition. Each color in the map correspond to a synchronization state between four MTJ oscillators and two input signals. Reproduced with permission.[58] Copyright 2018, Springer Nature.

© 2023 The Authors. Advanced Materials published by Wiley-VCH GmbH

15214095, 0, Downloaded from https://onlinelibrary.wiley.com/doi/10.1002/adma.202205047, Wiley Online Library on [19/06/2023]. See the Terms and Conditions (https://onlinelibrary.wiley.com/terms-and-conditions) on Wiley Online Library for rules of use; OA articles are governed by the applicable Creative Commons License

oscillators can generate a wide range of waveform patterns, which can be associated with another set of patterns, for example, horse gaits. The modulation of the synchronization has the potential to facilitate the motion control of a horse-like four-footed micro-robot.[25c,54b]

The abovementioned working mechanism of ONNs is highly consistent with Hopfield networks.[21a] The coupling type (in-phase or antiphase) between neurons corresponds to the positive or negative synaptic weight; the nonlinearity of the synchronization process brings the sigmoidal activation function; and the phase pattern of synchronization acts as the output state with the minimum energy. Such similarity makes ONNs suitable for solving optimization problems. Moreover, a level-based Hopfield network typically needs a number of iterations to reach the minimum energy. In each iteration, we need to calculate the system energy and the input for the next step. However, this optimization process can be naturally finished by an ONN over the course of relaxation to the equilibrium state. Parihar et al. built ONNs based on VO_2 oscillators to solve graph coloring problems, as shown in **Figure 7**.[25a] The nodes of an undirected unweighted graph are represented by neurons, and the edges connecting these nodes are represented by capacitive coupling between the neurons. Figure 7a shows the circuit schematic of four coupled neurons with capacitive connections. By controlling the transistors, this circuit can emulate four-node undirected graphs defined by arbitrary adjacency matrices. Note that the adjacency matrix can also be used to calculate the energy of a level-based Hopfield network. Capacitive coupling tends to generate a maximum phase difference. Due to the interconnection between multiple neurons, the phase difference between neurons would coordinate with each other to reach a steady global maximum. Figure 7b shows a four-node fully interconnected graph and the final oscillation waveforms of the neurons in the corresponding ONN. Calculating the average XOR values of the output waveforms of neurons can divide them into different groups, which gives the solution to the graph coloring problem. Using this method, ONNs corresponding to various graph configurations are experimentally demonstrated and the results are shown in Figure 7c.

From Figure 7a, we can see that the coupling of neurons in an ONN can be described by a binary symmetrical matrix. Such a matrix serves as a convenient analog to the Ising model which consists of binary variables to represent magnetic dipole moments or atomic spins.[61] Dutta et al.[25b] implemented an Ising Hamiltonian solver using eight coupled neuronal oscillators. The non-zero matrix elements of an 8×8 Ising Hamiltonian (**Figure 8**a) which depicts the interaction between eight atoms can be emulated by the capacitive coupling

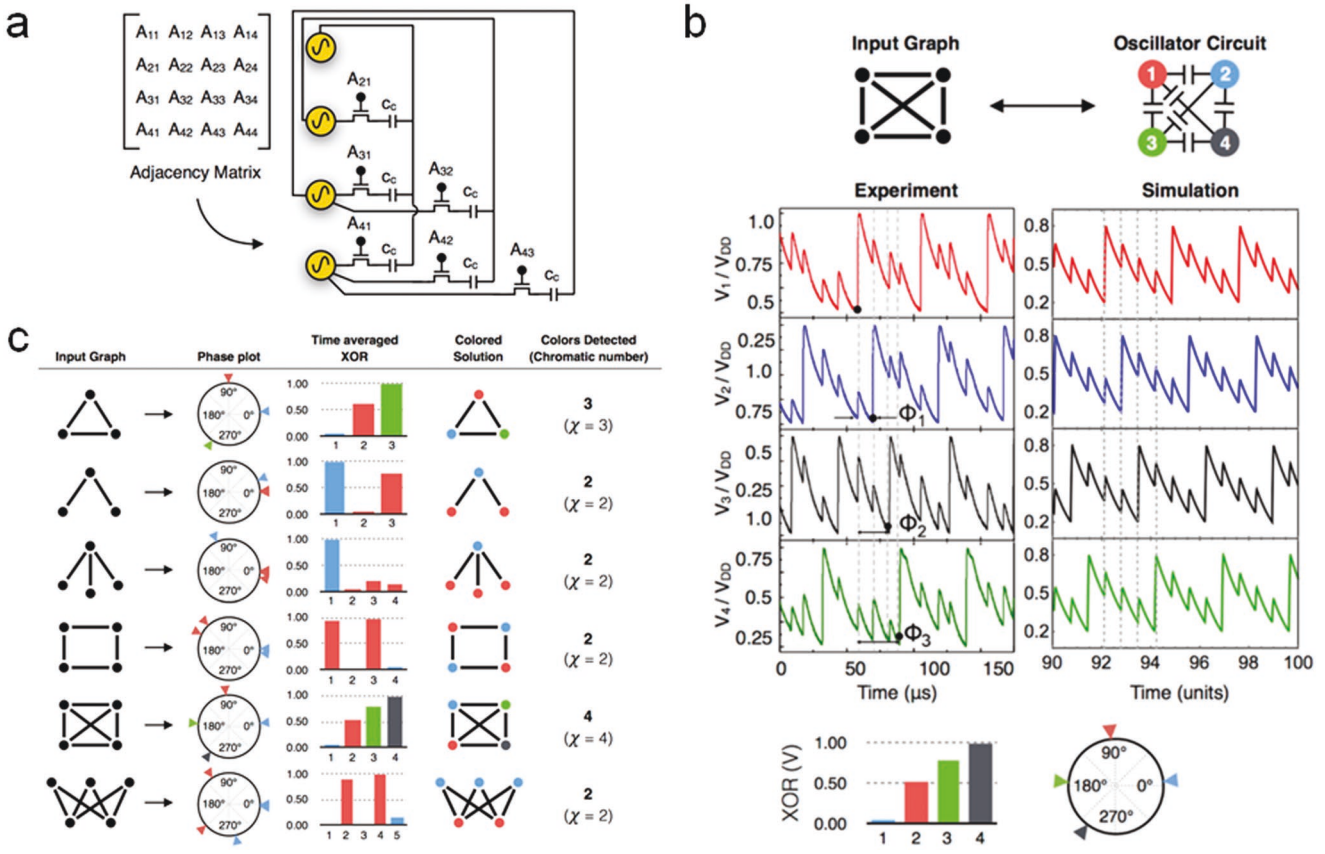

Figure 7. An ONN to solve graph coloring problems. a) The circuit schematic of four coupled oscillators for representing four-node undirected graphs defined by arbitrary adjacency matrices. Note that $A_{ij} = A_{ji}$, $A_{ii} = 0$ and $A_{ij} = 0$ or 1. b) The waveforms of four fully coupled oscillators after reaching synchronization. Time averaged XOR values of oscillation outputs give the solution to the problem. c) Experimental results of graph coloring using ONNs corresponding to various graph configurations. Reproduced with permission.[25a] Copyright 2017, Springer Nature.

© 2023 The Authors. Advanced Materials published by Wiley-VCH GmbH

15214095, 0, Downloaded from https://onlinelibrary.wiley.com/doi/10.1002/adma.202205047, Wiley Online Library on [19/06/2023]. See the Terms and Conditions (https://onlinelibrary.wiley.com/terms-and-conditions) on Wiley Online Library for rules of use; OA articles are governed by the applicable Creative Commons License

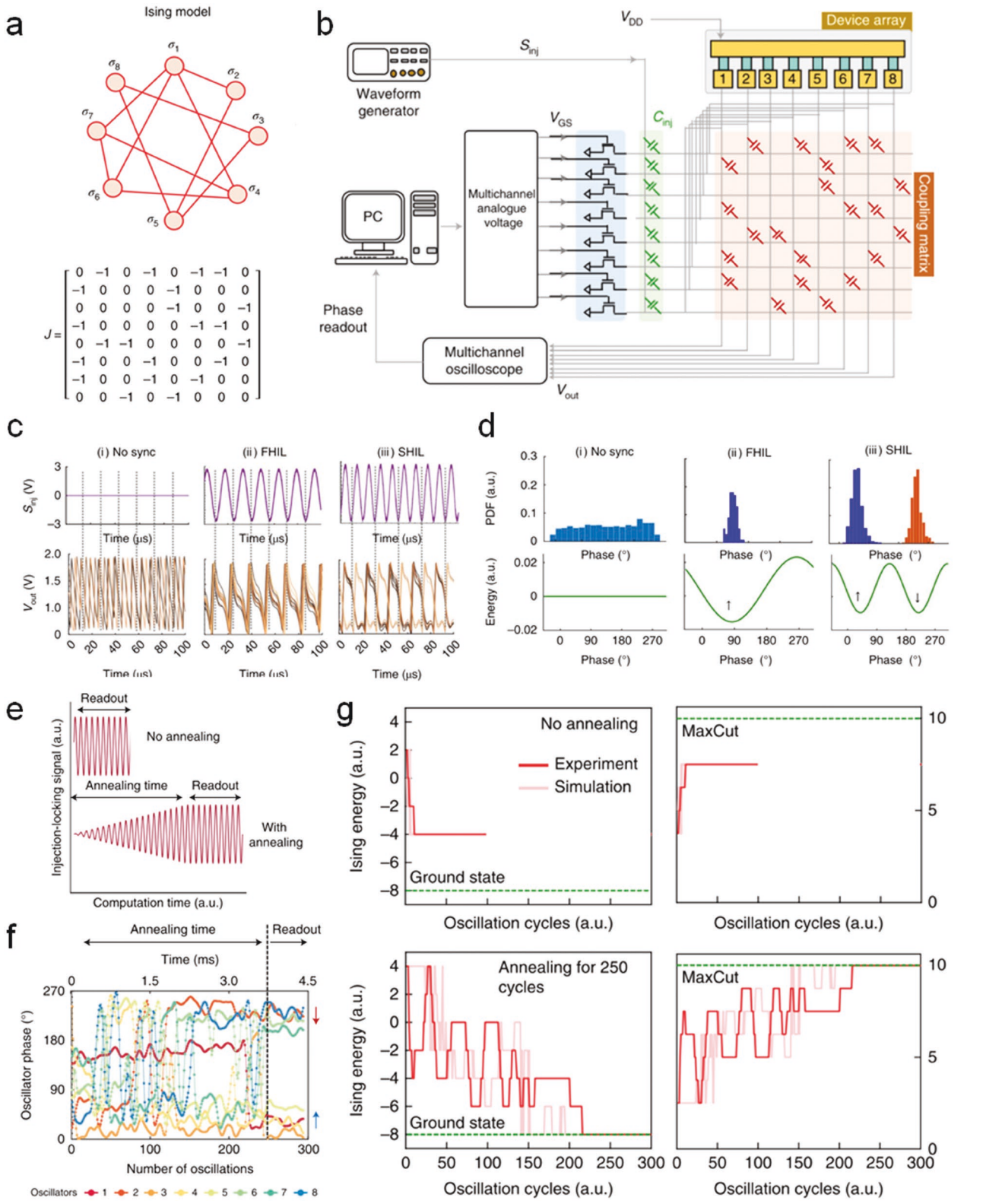

Figure 8. An Ising Hamiltonian solver based on coupled VO_2 neuronal oscillators. a) An eight-node Ising model and b) the hardware setup of corresponding ONN. Each non-zero matrix elements of the 8 × 8 Ising Hamiltonian corresponds to a capacitive connection between two neurons in the ONN. c) Measured oscillation waveforms and d) the phase distribution of three different injection-locking scenarios, (i) no synchronization, (ii) first-harmonic injection-locking, and (iii) second-harmonic injection-locking. e) Schematic of the annealing schedule used in the experiment. f) Phase evolution of the eight neurons, settling to either the in-phase or out-of-phase configuration after synchronization. Two neuron groups (1, 3, 4, 5) and (2, 6, 7, 8) represent the optimal solution of the MaxCut problem. g) Comparison of the energy evolution and optimization result obtained without or with the annealing schedule. Reproduced with permission.[25b] Copyright 2021, Springer Nature.

© 2023 The Authors. Advanced Materials published by Wiley-VCH GmbH

15214095, 0, Downloaded from https://onlinelibrary.wiley.com/doi/10.1002/adma.202205047, Wiley Online Library on [19/06/2023]. See the Terms and Conditions (https://onlinelibrary.wiley.com/terms-and-conditions) on Wiley Online Library for rules of use; OA articles are governed by the applicable Creative Commons License

between the corresponding neurons in the ONN (Figure 8b). The bound state of the system with minimum energy can be derived from the phase of neurons after synchronization. To equip each neuron with a binary degree of freedom to encode spin-up and spin-down states, a sinusoidal injection locking signal (S_{inj} in Figure 8b) at twice the oscillator intrinsic frequency is applied to the neurons. As shown in Figures 8c[iii] and d[iii], due to the second-harmonic injection-locking (SNIL) phenomenon, the oscillator waveforms after synchronization show both in-phase (40°) and antiphase (220°) injection-locking configuration, corresponding to up-spin and down-spin, respectively. Using SNIL, both ferromagnetic and antiferromagnetic interactions are replicated by the ONN. The researchers also investigated the performance of the ONN on a NP-hard problem of MaxCut for an eight-node undirected and unweighted graph, that is, to cut the graph into two subsets, such that the number of edges connecting the two subsets is maximized. This problem can be solved by the ONN because, for a given connection matrix, maximizing cut size is mathematically equivalent to minimizing Ising Hamiltonian. To enhance the success rate of converging to the optimal solution, a simulated annealing process is applied by gradually increasing the amplitude of S_{inj} (Figure 8e) so that the intrinsic stochasticity of the neuronal oscillator can help the optimization result escape from local minima. Figure 8f shows the phase evolution of the eight neurons over the optimization process. After synchronization, eight neurons will settle to either the in-phase or antiphase state and naturally form two groups, which represent the optimal graph cut. Figure 8g compares the energy evolution and optimization result obtained without or with the annealing schedule. Annealing over 250 oscillation cycles allows the network to converge to the optimal solution with higher probability.

2.2. Leaky Integrate-and-Fire Artificial Neurons

The LIF neuron model captures the general procedures of neural spike train transformation. The MP is not predetermined but evolves with input currents. Any arriving input spikes push up the MP until it reaches the threshold, at which point an output spike is generated, and the MP is reset to its resting potential. The increased MP would spontaneously decay if it does not reach the threshold, which can be represented as the "leak" term in addition to the derivative form of the law of capacitance:

$$C_m \frac{dV_m(t)}{dt} = I(t) - V_m(t) G_m \quad (1)$$

C_m and G_m are the capacitance and conductance of the neuron membrane. $V_m(t)$ and $I(t)$ are the MP and the total input current at time t.[62] To accurately mimic the LIF behavior, the time constant of the spontaneous decay $\tau = \frac{C_m}{G_m}$ and the mean arrival time of input pulses Δt_0 should be comparable. If $\tau \ll \Delta t_0$, the elevated MP will be discharged so fast that the neuron can hardly fire. If $\tau \gg \Delta t_0$, the leak effect will be too weak to eliminate the impact of long-past input spikes, and the neuron becomes an integrate-and-fire (IF) neuron.[63]

2.2.1. Device Mechanisms

The LIF behavior is typically demonstrated by applying a pulse train to threshold switching devices. An inherent relaxation process of the employed switching device is required. As discussed before, the working frequency range depends on the characteristic frequency $f_0 = \frac{G_0}{2\pi C_0}$, which is determined by the parasitic capacitance (C_0) and conductance (G_0) of the switching device. Considering C_0 is usually very small, an auxiliary circuit consisting of a capacitor and an optional transistor (or resistor) is usually added to regulate the operating frequency, as shown in **Figure 9**a. More circuit designs can be used to further tune the LIF behavior (Figure 9b–d). Assisted by the leaky integrator circuit, the MP evolution of LIF neurons based on IMT oscillators,[24b] ovonic threshold switching devices,[34,64] volatile memristors,[43a,65] van der Waals (vdW) material-based volatile memristors,[66] and HZO or PZT FeFETs[13a,c] have been captured. The LIF dynamic is also demonstrated using MTJ oscillators with a more complicated peripheral circuit which involves a reference MTJ.[67]

The MP is not necessarily represented by a voltage level, but can also refer to the progress of a physical or chemical process that leads to an electrical switching, such as phase transition, ion migration, and conductive filament growth (**Figure 10**). In these cases, the auxiliary capacitor is not required anymore, which can largely enhance the area efficiency of neuronal devices. As mentioned in Section 2.1.2, a single spike input to a Mott insulator converts a small part of it to a metastable correlated metal state. The effect gets accumulated as more pulses arrive and finally leads to the threshold switching. The spontaneous relaxation from the metastable intermediate state to the stable state accounts for the leaky mechanism.[42a] Similar scenario also applies to the LIF neurons based on VCM[68] and ECM memristors,[31,33,65d,69] and electrolyte-gated transistors.[70] In order to obtain a robust switching and relaxation process, engineering methods such as incorporating silver nanoparticle[9c] or nitrogen doping[71] to the switching media of memristors have been developed to modify the switching process. In magnetic devices, the LIF dynamics can be emulated by manipulating the partial volatile magnetization of ferromagnetic films,[17a,72] the domain walls in MTJs,[73] or the motion of a magnetic skyrmion.[12a–c] Some reported devices are IF neurons without a leak mechanism. For example, the intermediate states of PCM neurons have a very long lifetime;[10a,b] the memristive neurons based on SiO_x nanorods or single layer MoS_2 exhibit very noisy fluctuation of MP during accumulation.[27b,69b]

Table 3 summarizes the characteristics of representative physical implementations of IF and LIF neurons. For a fair comparison, some reported artificial neuronal devices that are based on non-volatile switching are not listed in the table, because they require additional reset operations to switch back to the resting potential and therefore are not regarded as complete neuronal devices.[12c,68a,69a,75]

2.2.2. Neuronal Dynamics

The LIF model involves the integration capability and the short-term memory. Therefore, it can cover more dynamics

© 2023 The Authors. Advanced Materials published by Wiley-VCH GmbH

15214095, 0, Downloaded from https://onlinelibrary.wiley.com/doi/10.1002/adma.202205047, Wiley Online Library on [19/06/2023]. See the Terms and Conditions (https://onlinelibrary.wiley.com/terms-and-conditions) on Wiley Online Library for rules of use; OA articles are governed by the applicable Creative Commons License

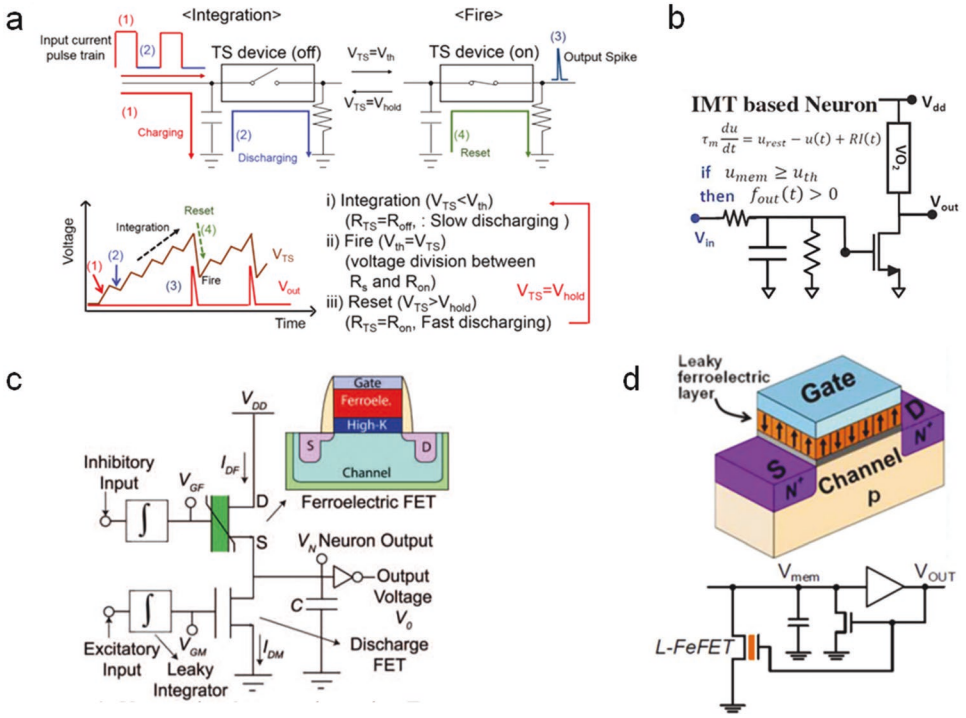

Figure 9. LIF neuron circuits with an auxiliary capacitor. a) A typical capacitor-based "leaky integrator" circuit for general threshold switching (TS) devices and its working mechanism. Reproduced with permission.[64a] Copyright 2019, Wiley-VCH GmbH. b) An alternative circuit design to enable LIF behaviors. The MP is the gate voltage of a transistor. Reproduced with permission.[3a] Copyriht 2020, AIP Publishing. c,d) Circuit designs for FeFET-based LIF neurons. Neuronal inhibition and frequency adaption are demonstrated using the two circuits, respectively. Reproduced with permission.[13a,c] Copyright 2018, IEEE, and 2019, IEEE.

of biological neurons. Spatial-temporal integration and refractory period are two features shared by most LIF neurons. Input spikes from different synapses are integrated to a LIF neuron and the temporal correlation between them can be processed by the leaky mechanism. Once the MP reaches the threshold, the hillock membrane of a LIF neuron will not respond to the input spikes over the course of firing and relaxation, which corresponds to the absolute refractory period of biological neurons.[64a,65c,66b,71]

Besides, two more advanced neuronal dynamics, neuronal inhibition and frequency adaption, are realized via circuit and operation design of FeFET neurons. As shown in Figure 9c, the neuron circuit has both excitatory and inhibitory input terminals which are the gate of the regular MOSFET and that of the FeFET, respectively. Pulses applied to the excitatory input increase the conductivity of the MOSFET and gradually pull down the V_S (the output voltage). Therefore, the V_{GS} of the FeFET will be elevated until it exceeds the threshold of ferroelectric polarization flip. The FeFET will be turned on, pull up the V_S, and induce the reverse ferroelectric transition. More input excitatory pulses will pull down the V_S again. Repeating this cycle will form a continuous neural spike train. However, if pulses are applied to the inhibitory input, the FeFET will stay in its on-state and hold the V_S at a relatively high level. Therefore, the excitatory pulses will only slightly pull down the V_S so that the V_{GS} of the FeFET is not large enough to trigger the ferroelectric switching. In other words, the neuron circuit gets inhibited.[13a] A leaky-FeFET-CMOS hybrid neuron as shown in Figure 9d was reported to experimentally demonstrate the spike frequency adaption.[13c] The key design for realizing spike frequency adaption is a leaky-FeFET with pulse accumulation effect and spontaneous polarization degradation as the discharge channel. During the neuron firing a spike, the ferroelectric switches and the current passing through the channel of the FeFET becomes larger. After switching back, the conductivity of the leaky-FeFET will be increased slightly due to the accumulation effect, and the V_{mem} in Figure 9d will be discharged faster. Therefore, it will take more input pulses to generate the next spike. The interspike interval continues to increase during the first few spikes. In the end, spontaneous ferroelectric polarization degradation will offset the accumulation effect and the interspike interval will settle to a constant value, leading to the spike frequency adaption. Simulation shows that another neuron design of a FeFET, together with six MOSFETs, can also realize the spike frequency adaption.[49]

Stochasticity is universally observed in LIF neurons with all kinds of device mechanisms. Though the differential Equation (1) seems linear, random variation exists in the $I(t)$ term even for LIF neurons driven by a very uniform pulse train. The response of MP to input pulses is intrinsically stochastic. The nonlinearity is even more significant for the LIF neurons whose MP evolution is associated with physicochemical processes.[66c,69b,71] Detailed statistical studies on some types of LIF neurons show that the number of spikes to trigger the firing approximately follows a Poisson distribution, and the probability of firing has a sigmoidal dependence on the

© 2023 The Authors. Advanced Materials published by Wiley-VCH GmbH

15214095, 0, Downloaded from https://onlinelibrary.wiley.com/doi/10.1002/adma.202205047, Wiley Online Library on [19/06/2023]. See the Terms and Conditions (https://onlinelibrary.wiley.com/terms-and-conditions) on Wiley Online Library for rules of use; OA articles are governed by the applicable Creative Commons License

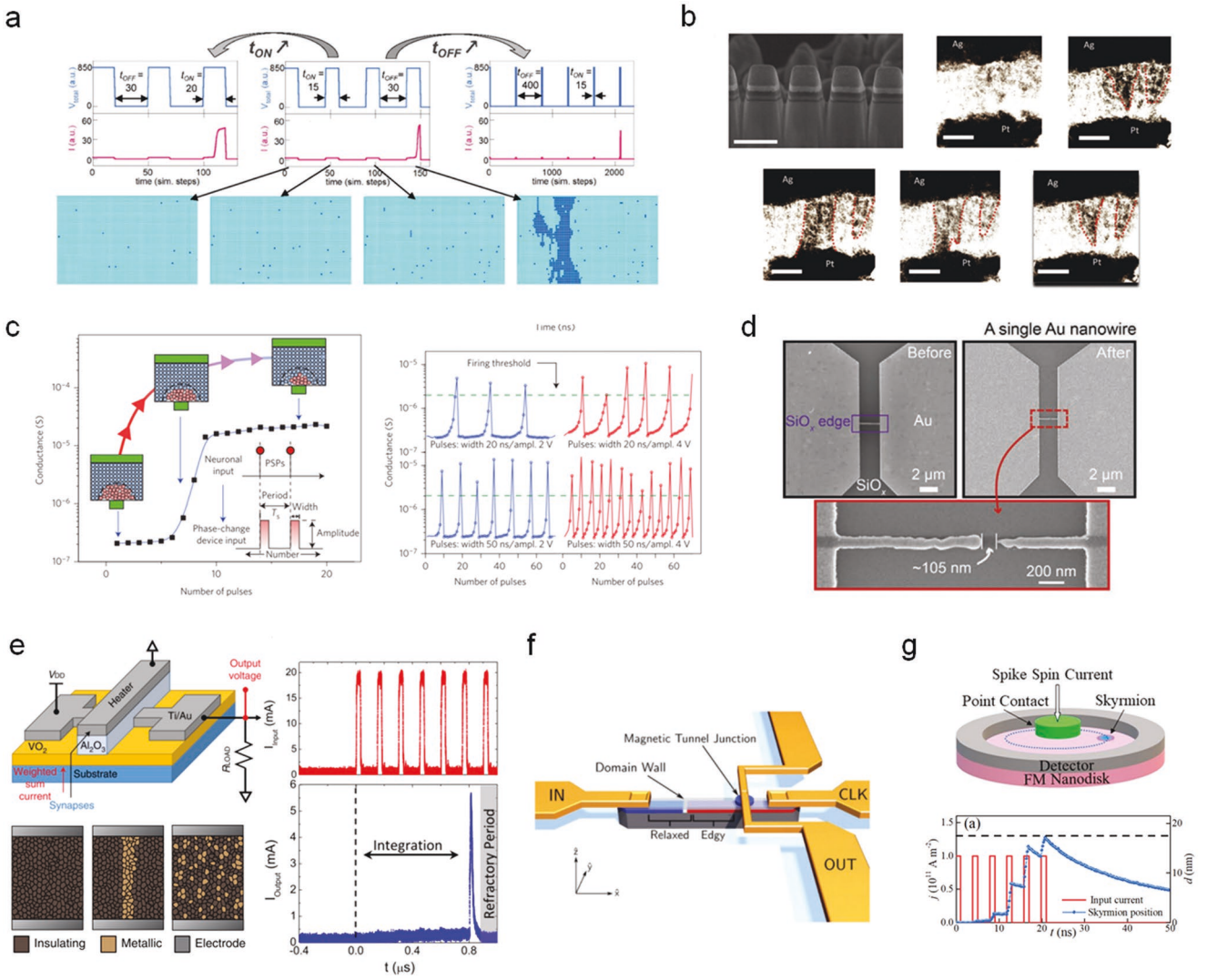

Figure 10. Device mechanisms of capacitor-free LIF neurons. a) Schematics of a Mott insulator that partially transitions to a metastable metal state while receiving a pulse train and finally forms a volatile conductive pathway. Reproduced with permission.[42a] Copyright 2017, Wiley-VCH GmbH. b) In situ transmission electron microscopy (TEM) images of the formation and spontaneous rupture of a silver conductive bridge in a FeO_x ECM memristor. Reproduced with permission.[65d] Copyright 2018, Wiley-VCH GmbH. c) The schematic evolution of the amorphous region of a PCM cell while receiving a pulse train and its LIF behavior. Reproduced with permission.[10a] Copyright 2016, Springer Nature. d) The scanning electron microscopy (SEM) images of the Au nanowires and nanogaps in a SiO_x nanorod memristive neuron. Reproduced with permission.[27b] Copyright 2021, Wiley-VCH GmbH. e) Schematics of a caloritronics-based Mott neuristor and its LIF behavior. Joule heating is employed to trigger the IMT transition of VO_2. Reproduced with permission.[74] Copyright 2020, Springer Nature, and 2021 Springer Nature. f) The schematic structure of an MTJ-based LIF neuron by manipulating the ferromagnetic domain walls. Reproduced with permission.[73a] Copyright 2021, IEEE. g) Schematics of a magnetic-skyrmion-based LIF neuron. The position of the skyrmion represents the MP. Reproduced with permission.[12c] Copyright 2020, AIP Publishing.

input pulse voltage.[31,65b] LIF neurons based on PCM or SiO_x nanorods are reported to show a Gaussian distribution of interspike intervals.[10a,27b] These results imply that the firing activity is approximately described by a Poisson point process, which agrees with the assumptions in mathematical theories for the neural spike train analysis.[76]

The stochastic properties and relatively low circuit complexity of LIF neurons enable the demonstration of novel probabilistic NC frameworks. The activity level distribution of a neuron population to the same stimulus can constitute PPC, which has been realized by PCM neurons.[10a,77] The thickness of the amorphous region and the internal atomic configuration vary from device to device. These features of a single device may also be changed after a switching cycle. Thus, the number of pulses (interspike interval) needed to generate a neural spike is random for individual devices. However, the interspike intervals of a group of phase change neurons have a relatively stationary distribution for a certain operation pulse width (**Figure 11**a), which is the PPC. Reversely, this statistical distribution of firing frequency of the neuron group serves as a good index of the underlying operating pulse width, and the representation error can be suppressed by a larger population size (Figure 11b). As a demonstration of frequency detection, the researchers varied the operating pulse width (tens

© 2023 The Authors. Advanced Materials published by Wiley-VCH GmbH

15214095, 0, Downloaded from https://onlinelibrary.wiley.com/doi/10.1002/adma.202205047, Wiley Online Library on [19/06/2023]. See the Terms and Conditions (https://onlinelibrary.wiley.com/terms-and-conditions) on Wiley Online Library for rules of use; OA articles are governed by the applicable Creative Commons License

15214095, 0, Downloaded from https://onlinelibrary.wiley.com/doi/10.1002/adma.202205047, Wiley Online Library on [19/06/2023]. See the Terms and Conditions (https://onlinelibrary.wiley.com/terms-and-conditions) on Wiley Online Library for rules of use; OA articles are governed by the applicable Creative Commons License

Table 3. Comparison of LIF neurons based on different device mechanisms.

Materials	Physics	Auxiliary circuit	Feature size F [μm][a)]	V_{in} [V][b)]	Operating current [mA]	Operating frequency	Neuron model	Reference
NbO_2	Mott transition	1R1C[c)]	4	1.3	0.8	≈1 MHz	LIF	[24b]
VO_2	Mott transition, Joule heating	1R (heater)	2	0.75	20	≈10 MHz	LIF	[74]
$GaTa_4Se_4$	Mott transition	1R	40	40	15	≈20 kHz	LIF	[42a]
$Ag/HfO_2/Ag$	ECM	1R1C	100	0.7	0.01	≈1 kHz	IF	[71]
SiO_x:Ag	Diffusive memristor	1R	2.5	0.8	1	≈10 kHz	IF	[43a]
Cu-Ta/IGZO/TiN	ECM	1R	50	4	10	≈1 kHz	LIF	[69f]
$Ag/FeO_x/Pt$	ECM	None or 1R	2	3.3	10	≈5 kHz	LIF	[65d]
SiO_x nanorod/Au	ECM	2R, 1 comparator	200	4	0.01	≈10 kHz	IF	[27b]
$TiN/Ti/HfO_2/TiN$	VCM	1T1C[c)]	10	3	0.01	≈100 kHz	IF	[68b]
$B_{0.25}Te_{0.75}$	Ovonic threshold switching	1R1C	0.03	0.3	0.025	≈0.45 MHz	LIF	[64a]
$Ge_2Sb_2Te_5$	PCM	1R	0.5	1.5	0.15	≈10 MHz	IF	[10a]
HZO	FeFET	1T1R	/[d)]	2	/	≈20 Hz	LIF	[13c]
PZT	FeFET	2R1C	/	3.3	0.001	≈30 kHz	LIF	[13a]
FeB/MgO/CoFeB	MTJ	2T, 1 MTJ	0.1	1	0.5	≈1 GHz	LIF	[17a]
MoS_2	Electrolyte-gated FET	3R1C	>2	5	0.0001	≈5 Hz	IF	[66c]
MoS_2/Graphene	VCM	3R1C	10	8	0.1 to 1	≈5 kHz	LIF	[66b]
$Ag/MoS_2/TiW$	ECM (lateral)	None	10	2	0.001	≈2 kHz	LIF	[69b]
$Ag/MoS_2/Au$	ECM	2R1C	5	1.2	0.1	≈10 kHz	LIF	[66d]
$Te/TiTe_2/Pt$	ECM	None	5	1.1	0.2	≈0.4 MHz	LIF	[33]
Ag/Nafion/Au	ECM	2R1C	6	2	0.001	≈80 Hz	LIF	[69d]

[a)]Feature area = $F \times F$ μm^2; [b)]V_{in}: the input voltage to the device; [c)]R: resistor, T: transistor, C: capacitor; [d)]Not specified.

of nanoseconds) periodically and the number of neurons that fire at a certain frequency shows a synchronized evolution pattern (Figure 11c), which means the pulse width at MHz level can be represented by neuronal firing behaviors at kHz level. Therefore, the Nyquist–Shannon theorem which defines the theoretical frequency detection limit was bypassed.[10a] In addition to this work, it is worthwhile to note that PPC can also be demonstrated using a group of synaptic devices, for example, MoS_2 synapses.[78]

Besides, psychophysical experiments indicate that human brains perform Bayesian inference in perception and decision making tasks.[79] In Bayesian inference, the information is encoded by probability distribution. Prior probability that represents existing knowledge is updated by new evidence to form posterior probability. Bayes' theorem defines the updating rule. Debashis et al. reported a two-node BN based on spintronic devices, and proposed the potential to scale up the network.[27a] Choi et al. built a BN based on SiO_x nanorod memristive neurons with tunable probabilistic activation functions.[27b] Pulse trains with different widths can control the probability distribution of the resistive state of the SiO_x neurons. In the demonstration of a genetic regulatory network as shown in Figure 11d, pulses with widths of 100 and 270 μs are applied to the neuron to represent the prior probability of G_1 expression, which are set to $P_{prior}(G_1 = T) = 0.2$ and $P_{prior}(G_1 = F) = 0.8$ (Figure 11e). A pulse train with 20% occupied by pulses and 80% by no pulse is used to represent $P_{prior}(G_1 = T)$, and its complementary pulse train represents $P_{prior}(G_1 = F)$. If another gene expression, for example, G_2 occurs, Bayesian inference can be done using the BN consisting of an edge circuit and a peripheral circuit, as proposed by the researchers. The two pulse trains related to the prior of G_1 are applied to the edge circuit of G_2 to obtain pulse trains corresponding to $P(G_2 = T)$ and $P(G_2 = F)$. Then, pulse trains of $P_{prior}(G_1 = T)$ and $P(G_2 = T)$ are input to a peripheral circuit to obtain a pulse train for $P_{post}(G_1 = T|G_2 = T)$, which is the posterior probability derived from Bayesian inference. Following this method, the researchers demonstrated the probabilistic inferences for four selected cases via simulation (Figure 11f).[27b] This work provides some reference about the operation framework and circuit design of BNs based on stochastic neuronal devices.

2.2.3. Spiking Neural Networks

SNNs are ANNs that closely follow the principles of biological nervous systems.[21b] In an SNN, neural spike trains are generated and transformed by the spiking neurons connected by synapses. During this process, the connection strength (synaptic weight) is updated according to synaptic plasticity. The processing results are stored in the updated weight of synapses.[19a] The LIF neuron is the most prominent neuron model to implement SNNs. Some reports show even a single LIF neuron can fulfill computing tasks like correlation detection with the help from software.[10a,80]

© 2023 The Authors. Advanced Materials published by Wiley-VCH GmbH

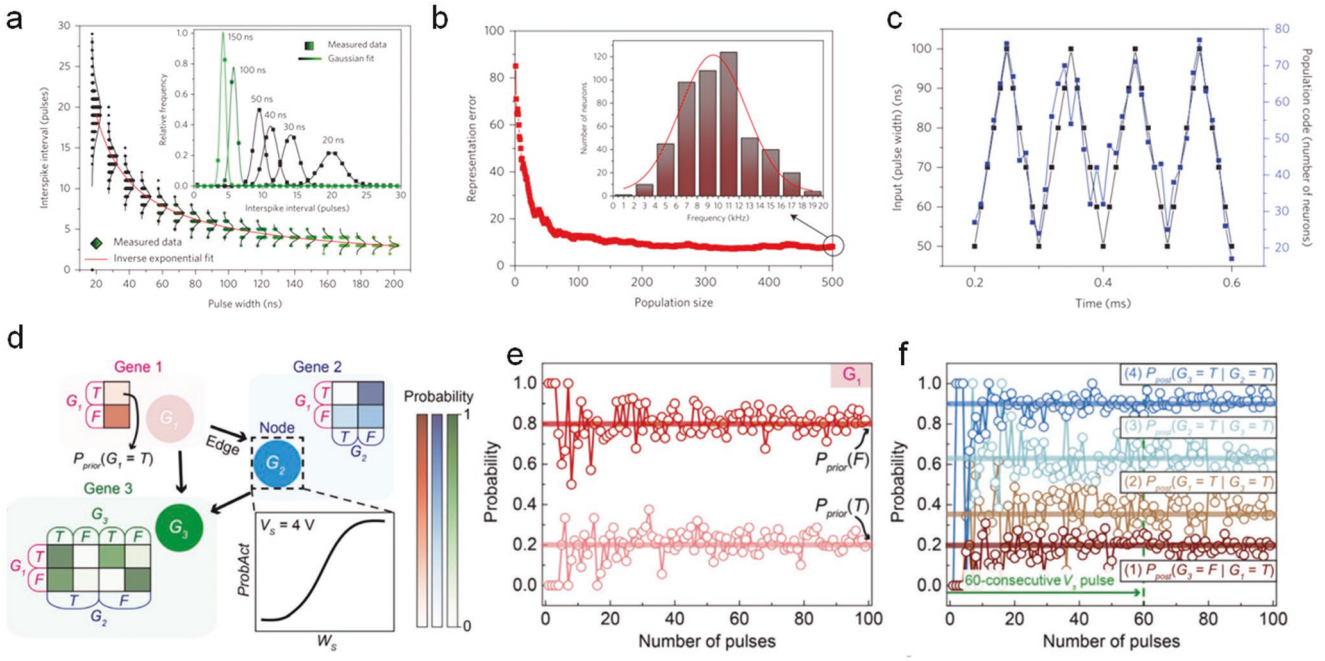

Figure 11. Experimental demonstration of probabilistic neuromorphic computing. a–c) Probabilistic population coding (PPC) demonstrated using stochastic PCM neurons. Reproduced with permission.[10a] Copyright 2016, Springer Nature. a) The distribution of interspike intervals in a single neuron excited by pulses of different widths. b) Error in the representation of the input stimulus using the population code. The stimulus is a triangular signal with a period of 0.1 ms and pulse width changes in the range of 50–100 ns periodically. Inset: For 500 neurons, the distribution of the actual spiking frequency across the neuron population when the input stimulus is applied. c) The time evolution of input pulse width (black) and population code for 500 neurons (blue). d,e) Probabilistic Bayesian inference demonstrated using SiO_x nanorod memristive neurons. Reproduced with permission.[27b] Copyright 2021, Wiley-VCH GmbH. d) A genetic regulatory network where the genes and regulatory directions are represented as the nodes and edges. The conditional probability boxes (red, blue, and green boxes) show the preset prior probability (P_{prior}) for Genes 1–3 ($G_{1–3}$). The inset graph shows the plot of the activation probability of the artificial neuron, which can be utilized as each node of the BN. e) Plots of the $P_{prior}(G_1 = T) = 0.2$ and $P_{prior}(G_1 = F) = 0.8$ based on the activation probability of the neuronal device operated with pulses of 100 and 270 µs widths, respectively. f) Probabilistic inference results, posterior probability (P_{post}) for four selective cases, 1) $P_{post}(G_3 = T|G_1 = T)$, 2) $P_{post}(G_1 = T|G_3 = T)$, 3) $P_{post}(G_2 = T|G_3 = T)$, and 4) $P_{post}(G_3 = T|G_2 = T)$ based on the BN consisting of the fabricated SiO_x memristive neurons.

In 2018, Wang et al. demonstrated the hardware implementation of a fully memristive SNN based on Pt/Ag/SiO_x:Ag/Ag/Pt diffusive memristor neurons and non-volatile Pd/HfO_x/Ta drift memristor synapses.[24a] The SNN consists of an 8 × 8 memristive synapse crossbar array and eight artificial neurons integrated to each column of the array. **Figure 12**a shows the optical micrograph of the SNN, and the scanning electron microscopy (SEM) and transmission electron microscopy (TEM) images of the synaptic and neuronal devices. Pattern classification of four letters was demonstrated using the SNN with pre-programmed synaptic weights which can be derived from an offline training process. Each column of synapses serves as a convolutional filter corresponding to a certain subimage pattern. The diffusive memristor neurons play the role of information integrators with a rectified linear unit (ReLU) activation function. The features of the input subimages can be revealed by the firing activity of their corresponding neurons. On top of that, an unsupervised learning process was demonstrated using a simple STDP rule using an 8 × 3 network (Figure 12b). In each iteration, one of the outputs of neurons in the abovementioned pattern recognition job were input to the untrained network, and the synaptic weights were updated using a lateral inhibition manner if any of the three neurons fires. Figure 12c shows the input voltage vector, the integrated neuron current, and the evolution of synaptic weights of each iteration. After the unsupervised learning, the network can classify the images of four letters into three groups. This work provides a valuable tutorial about the peripheral circuit design and algorithm realization for hardware implementation of SNNs.

Duan et al. reported a 4 × 4 SNN consisting of NbO_x-based neurons and non-volatile TaO_x memristor-based synapses.[24b] Figure 12d shows the SEM and TEM images of Pt/Ti/NbO_x/Pt neurons and Pt/Ta/TaO_x/Pt synapses. The SNN was also applied to pattern classification of four-pixel black-and-white images. The weights of synapses are programmed to desired values through offline training. Besides the information integration and activation function, the NbO_x neurons show frequency response to different excitation inputs, owing to the frequency dependence feature of IMT neurons. Furthermore, supervised online learning was performed on the SNN. Figure 12e shows the schematic of supervised learning. The synaptic weights were updated by the feedback circuit based on simplified δ-rule, a type of gradient descent method for spiking neurons. Figure 12f shows the weight evolution of four synapses connected to a single neuron over the learning process. Similarly, Hao et al. reported a 4 × 2 SNN based on MoS_2 neurons and Cu/GeTe synapses with the capability of classifying even simpler images.[69b] Simulation and some initial experimental

© 2023 The Authors. Advanced Materials published by Wiley-VCH GmbH

15214095, 0, Downloaded from https://onlinelibrary.wiley.com/doi/10.1002/adma.202205047, Wiley Online Library on [19/06/2023]. See the Terms and Conditions (https://onlinelibrary.wiley.com/terms-and-conditions) on Wiley Online Library for rules of use; OA articles are governed by the applicable Creative Commons License

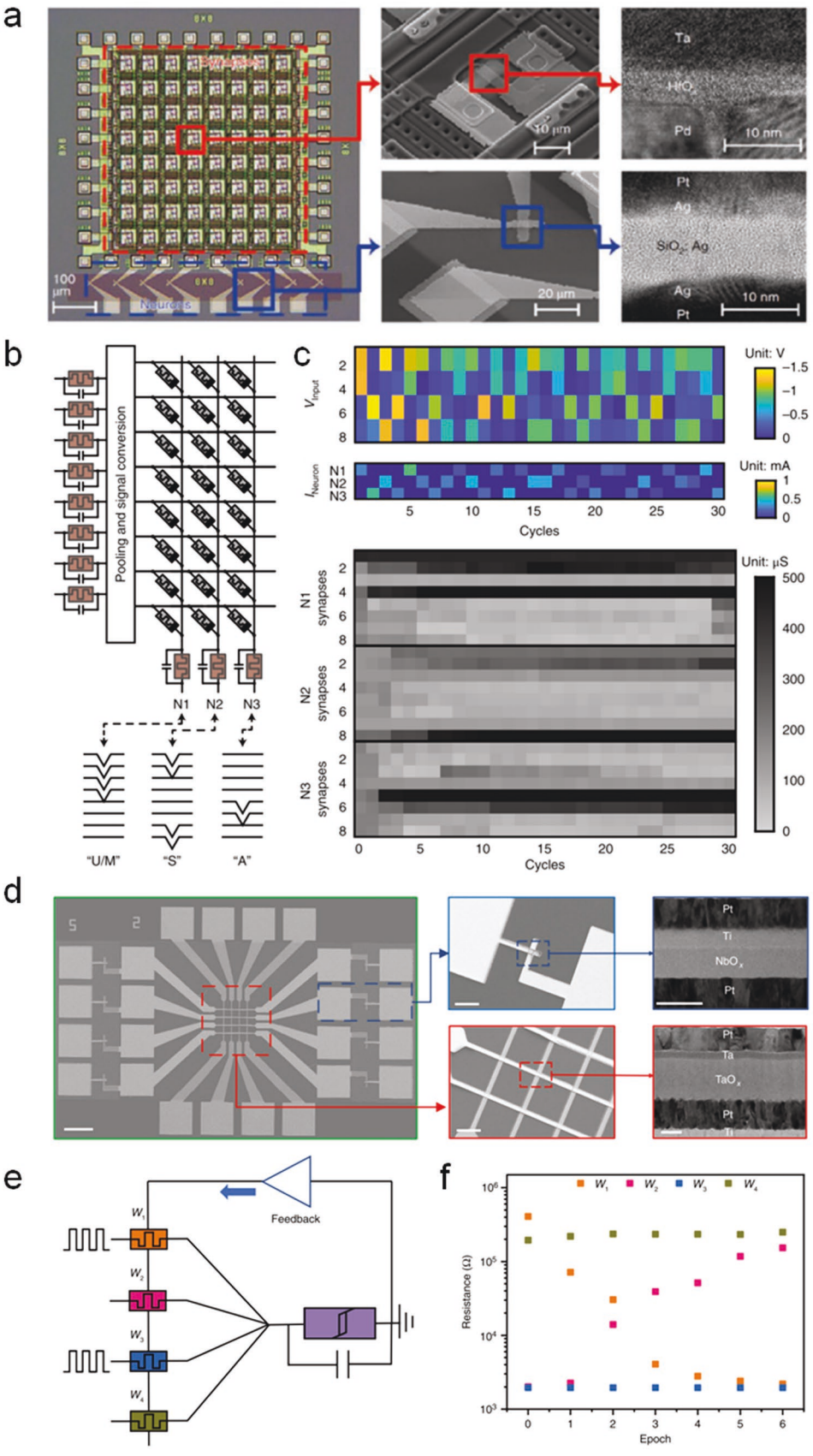

© 2023 The Authors. Advanced Materials published by Wiley-VCH GmbH

15214095, 0, Downloaded from https://onlinelibrary.wiley.com/doi/10.1002/adma.202205047, Wiley Online Library on [19/06/2023]. See the Terms and Conditions (https://onlinelibrary.wiley.com/terms-and-conditions) on Wiley Online Library for rules of use; OA articles are governed by the applicable Creative Commons License

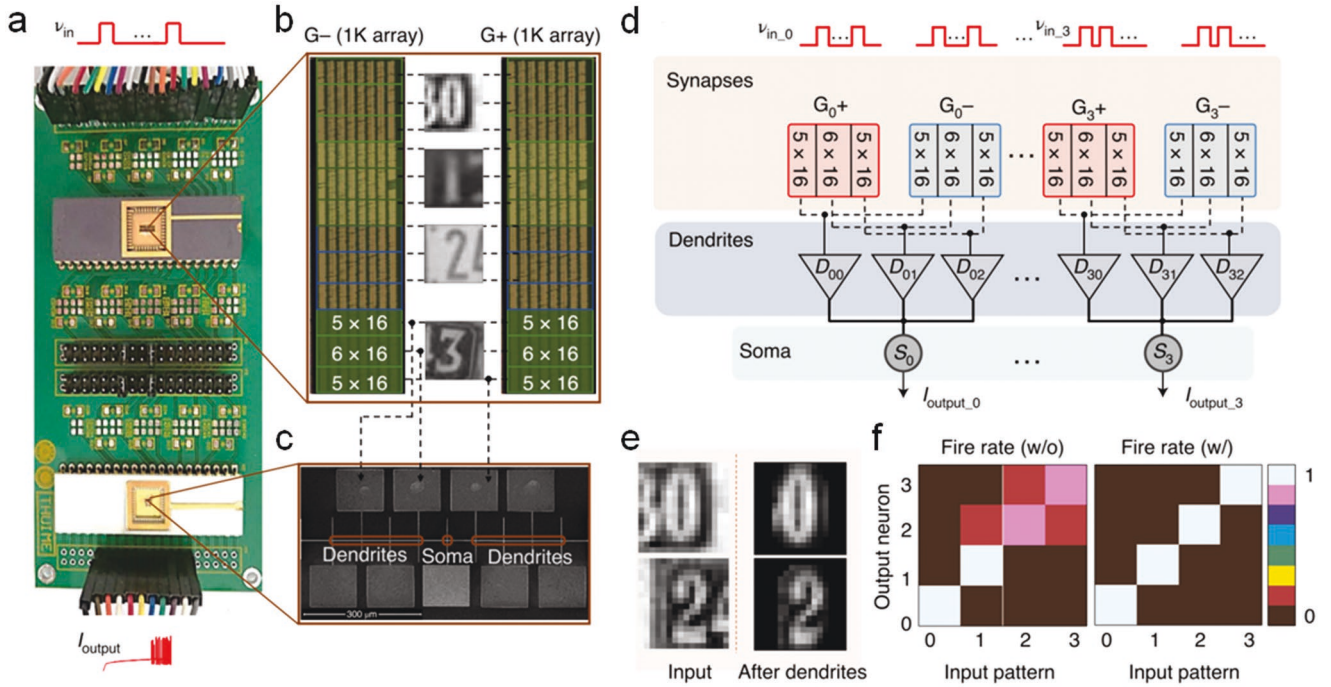

Figure 13. a) Optical image of a single-layer SNN circuit with artificial dendrites. b) Optical image of the synapse array. c) SEM image of a neuron with eight dendrites and one soma. d) Schematic structure of the SNN. e) Comparison between input images and processed images after dendrites in the neural network. f) Comparison of the neuron firing rates with and without the artificial dendrites. Reproduced with permission.[24c] Copyright 2020 Springer Nature.

results indicate that other LIF neuronal devices also have the potential, but more engineering efforts are still needed for their hardware implementation.[17a,49,64a,65b,c,66c]

Li et al. reported an SNN based on artificial neurons with multiple dendrites (**Figure 13**).[24c] A few of memristors with a $Pt/TaO_x/AlO_\delta/Al$ structure as artificial dendrites are connected to a NbO_x artificial soma. The AlO_δ layer serves as a reservoir to induce oxygen ion diffusion in the dendrite device. Applying electrical bias can control the oxygen ion distribution and thus tune the Schottky-like barrier between Pt and TaO_x. The dendrite devices can filter out small input signals in the off-state and nonlinearly integrate input signals in their on-state. The dendrite and soma devices were integrated to an array of $TiN/HfO_x/TaO_x/TiN$ synapses to form a single-layer SNN. The network was trained in software using a back-propagation algorithm for fulfilling digit recognition. The dendrite layer not only filtered the background noise in the input picture, but also highlighted the critical signals in the images, as shown in Figure 13e. The neuron firing rate caused by incorrect image inputs was suppressed by the additional dendrites (Figure 13f) so that the recognition accuracy was enhanced. Compared to systems without dendrites, the power consumption of soma was reduced by over 30 times in this SNN. However, because the dendritic unit itself consumed more than 50% of the total power, the overall energy cost was actually even higher.

It is worth noting that there are also hardware implementations of ANNs based on non-spiking neurons. Joule heating, instead of voltage bias, was employed to trigger the IMT switching of VO_2 neurons, which are also called caloritronics-based neuristors.[74a] Such a neuronal device features a ReLU activation function. A couple of this type of neurons is integrated with a crossbar of conductive bridge synapses to perform large-scale image edge detection.[74b]

2.3. Hodgkin–Huxley Artificial Neurons

Although LIF neurons capture a key aspect of neuronal functionality, the simplification prevents them from covering more details, such as the multiple stages of an action potential, and advanced neuron dynamics like subthreshold oscillation and inhibition-induced spiking. Emulating these behaviors requires a more accurate replication of the sophisticated structure and biophysical characteristics of neuronal membranes, especially

Figure 12. Hardware implementation of SNNs based on artificial neuronal devices integrated with synapse arrays. a) Optical micrograph, SEM, and TEM images of an 8 × 8 network consisting of $Pt/Ag/SiO_x$:Ag/Ag/Pt diffusive memristor neurons and $Pd/HfO_x/Ta$ drift memristor synapses. b) The schematic of an 8 × 3 network for unsupervised learning. c) The input voltage vector, the integrated neuron current, and the evolution of synaptic weights of each cycle in the unsupervised learning process. Reproduced with permission.[24a] Copyright 2018, Springer Nature. d) SEM and TEM images of an SNN consisting of $Pt/Ti/NbO_x/Pt$ neurons and $Pt/Ta/TaO_x/Pt$ synapses. e) The schematic illustration of the supervised online learning based on simplified δ-rule in this SNN. f) The weight evolution of four synapses connected to a single neuron over the learning process. Reproduced with permission.[24b] Copyright 2020, Springer Naure.

© 2023 The Authors. Advanced Materials published by Wiley-VCH GmbH

15214095, 0, Downloaded from https://onlinelibrary.wiley.com/doi/10.1002/adma.202205047, Wiley Online Library on [19/06/2023]. See the Terms and Conditions (https://onlinelibrary.wiley.com/terms-and-conditions) on Wiley Online Library for rules of use; OA articles are governed by the applicable Creative Commons License

the voltage-controlled ion channels.[81] HH neuron model is a mathematical model with better biological plausibility, which can be written as:

$$I(t) = C_m \frac{dV_m(t)}{dt} + G_K(V_m(t) - V_K) + G_{Na}(V_m(t) - V_{Na}) + G_L(V_m(t) - V_L) \quad (2)$$

where G_K, G_{Na}, and G_L are the conductance of potassium ions, sodium ions, and natural leakage, respectively, and V_K, V_{Na}, and V_L are the reverse potentials of potassium, sodium, and leakage, respectively.[82] The equivalent electrical circuit of HH model is shown in the middle part of Figure 1.

Theoretical research proposed that the HH dynamics can be implemented by memristive systems.[83] In 2013, Pickett et al. exploited the voltage-controlled phase transition of NbO_2 to emulate the opening and closing of potassium and sodium ion channels, as well as two DC voltage sources to generate the reverse potentials V_K and V_{Na} (**Figure 14**a).[8a] Careful design of the auxiliary passive components makes the switching of two equivalent ion channels follow the sequence of their biological counterparts. As a result, a biologically plausible action potential with different stages, namely, hyperpolarization, depolarization, and a refractory period, is simulated (Figure 14b). The capability of generating neural spike trains with different interspike intervals is also demonstrated (Figure 14c). Following this track, Yi et al. used another IMT material, VO_2, to experimentally demonstrate 23 biological spiking behaviors (Figure 14d,e), as well as characterizing capacitance-dependent operating regimes and stochastically phase-locked firing properties.[84] Some advanced behaviors such as burst firing mode, frequency adaption, and neuronal inhibition are expected play important roles in enabling energy-efficient neural processing,[7a,85] but the hardware demonstration of these dynamics remains rudimentary and relatively limited. The explicit function of other high-order behaviors, such as subthreshold oscillation and mixed firing mode, in neural signal processing remains largely uncovered. Some investigations have partially revealed the important role of HH neurons in enabling hierarchical learning and energy-efficient computing.[86]

To date, the hardware demonstration of HH neurons remains very rare. Although a quasi-HH neuron that uses a non-HH circuit is proposed to have the capability of generating spikes with similar MP evolution as a real action potential, its firing activity relies on the addition of a 555 timer integrated circuit, which severely increases the circuit complexity.[87] Furthermore, the application of HH neurons is mostly restricted to biological neuron emulation. Simulation shows that the HH-neuron-based circuits are capable of performing general Boolean logic operations, which proves the computational universality of HH neural networks.[88] A neuromorphic analog computing solution to a computationally hard graph-partitioning problem is

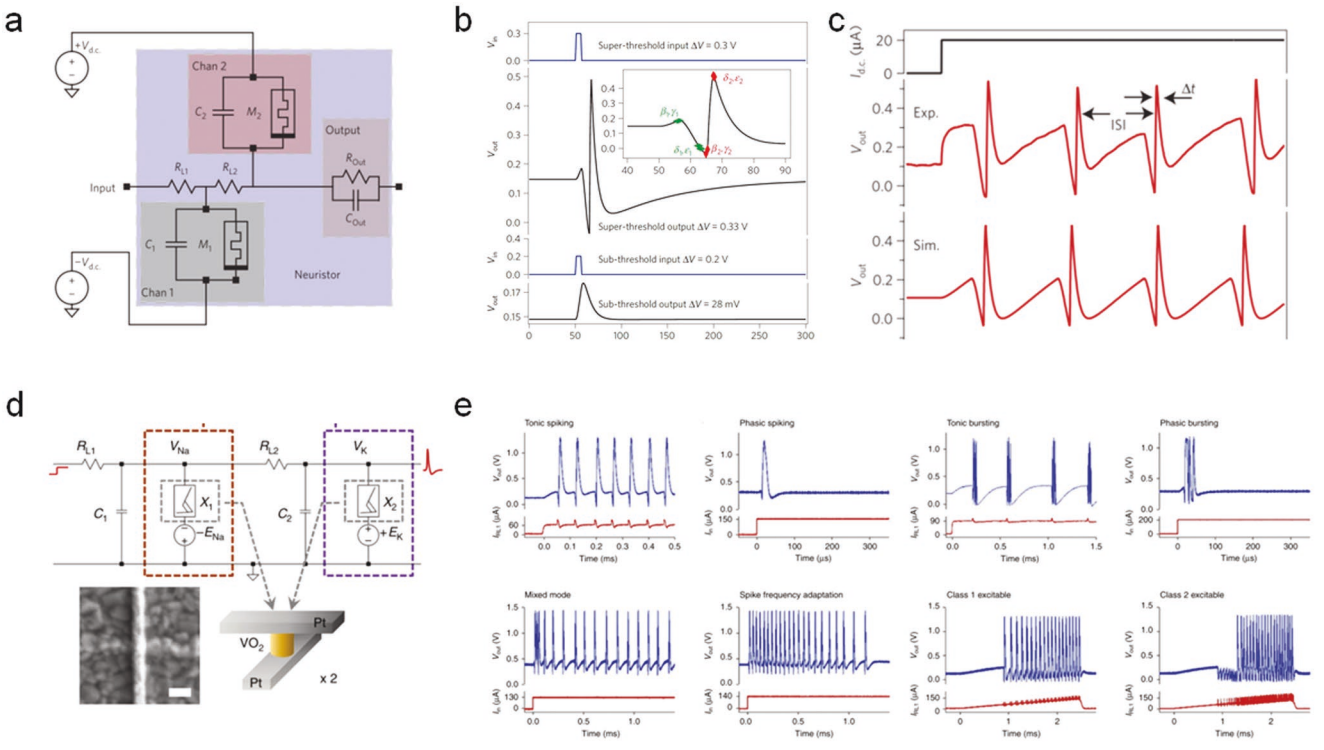

Figure 14. Demonstration of HH neurons and neuronal behaviors. a) Circuit diagram of the HH neuron. The channels consist of two NbO_2 Mott memristors (M_1 and M_2), each with a characteristic parallel capacitance (C_1 and C_2, respectively) and are biased with opposite polarity DC voltage sources. b) All-or-nothing response to super-threshold and sub-threshold input pulses. A super-threshold 0.3 V input pulse and its corresponding spike output (action potential). The magnified spiking region (inset) highlights the time sequence of events for channels one and two. A sub-threshold 0.2 V input to the same device yields an attenuated output. c) Experimental and simulated neural spike trains generated by the HH neuron. Reproduced with permission.[8a] Copyright 2012, Springer Nature. d) Circuit topology of a two-channel VO_2 active memristive neuron to emulate the HH neuronal dynamics, the schematic structure, and a SEM image of a typical VO_2 active memristor. e) A fraction of the 23 biological neuron spiking behaviors experimentally demonstrated in the VO_2 active memristor neurons. Reproduced with permission.[84] Copyright 2018, Springer Nature.

© 2023 The Authors. Advanced Materials published by Wiley-VCH GmbH

15214095, 0, Downloaded from https://onlinelibrary.wiley.com/doi/10.1002/adma.202205047, Wiley Online Library on [19/06/2023]. See the Terms and Conditions (https://onlinelibrary.wiley.com/terms-and-conditions) on Wiley Online Library for rules of use; OA articles are governed by the applicable Creative Commons License

proposed based on NbO_2 neurons with three dynamical electrophysical processes, which partially resemble the working mechanism of HH neurons.[89] However, computational applications that take full advantages of HH neuronal dynamics remain missing, which is largely attributed to people's limited knowledge about their role in the functionality of biological neurons.

3. Artificial Sensory Neurons

Besides implementing computational tasks, artificial neuronal devices can also be integrated with sensors to work as sensory neurons. In biological systems, sensory neurons are regarded as the first stage of data input in the interaction with the surrounding environment.[90] The massively collected data are filtered, integrated, and refined for dynamically training the neural network, which shapes our perception and understanding of the world around us.[91] Hence, the hardware implementation of sensory neurons is an important cornerstone of building artificial intelligent systems. Artificial sensory neurons that resemble the function of human eyes or skin have received much research interest in the past few years.

3.1. Visual Neurons

Mammalian visual system is capable of perceiving visual information and recognizing different targets in a complex environment.[92] Artificial visual perception systems are now gaining more research attention for they can potentially realize real-time pattern recognition with faster speed and higher efficiency.[93]

Various materials and device structure designs are deployed to achieve artificial visual perception. Most of the research focuses on photo-synaptic devices; however, these devices lack the complex function of mammalian retinal neurons.[94] Among the previously reported works on visual neurons, hybrid integration of a photoreceptor and a neuromorphic component, which functions as an optical signal sensor and a signal processor, respectively, is usually employed to construct the artificial visual system. Bao et al. reported a one-transistor-one-memristor structure to mimic the functions of photoreceptor cell and ganglion cell in human eyes. The changes in MP and neuronal spiking caused by photo-illumination can be mimicked by the voltage changes between the two terminals of the transistor and memristor. In their demonstration, the shape information of input images can be extracted and encoded as neural spikes for further processing.[95] To extend human vision to the ultraviolet (UV) band, oxide semiconductor IGZO is utilized as a UV sensor. By combining with a NbO_x memristor as the oscillation neuron, the IGZO/NbO_x system can detect the UV image information and convert it into neural spikes. The neural spike trains are then processed by a neural network. Image segmentation in a complex background was successfully implemented.[96] Similarly, by integrating organic near-infrared (NIR) photo synapses with Ag/SiO_2/Ag-based LIF neurons, Mu et al. constructed a vision sensory neuron.[97] Fundamental synaptic behaviors, like short-term plasticity, long-term plasticity, and paired pulse facilitation/depression, are mimicked by the NIR artificial synapse. The output of the NIR artificial neuron system is sent to a two-layer SNN and a test accuracy rate of 63.21% in the handwritten digit classification is achieved. However, the accuracy still has much room for improvement and the energy budget is still relatively high.

Recently, a photoelectric spiking neuron for visual depth perception was implemented based on a photoresistor and a TaO_x memristor-based spiking encoder, as shown in **Figure 15**a.[98] Figure 15b shows that the light stimulation pulse can be encoded into neural spikes by the LIF neuron with four critical neuronal behaviors: all-or-nothing spiking, threshold-driven spiking, a refractory period, and strength-modulated frequency response. The firing frequency is similar to that of biological neuron in the range of 1–200 Hz, with low energy consumption. Figure 15c exhibits the emulation of binocular vision based on the photoelectric spiking neuron system. This system demonstrates a recognition improvement by refocusing on sights with different distances, which resembles biological visual systems.

For the works stated above, the information perception units and data processing components are physically separate, which will inevitably cause data latency, high power consumption, as well as system complexity. To address this challenge, near-sensor and in-sensor computing paradigms are proposed to perform signal sensing, collection, and computing near or within the sensory device. A single phototransistor was recently proposed to mimic the retinal neuron with typical IF behaviors.[99] Neuronal firing is activated by electric stimuli and fire characteristics can be dynamically modulated by light stimuli. Image recognition is proved to be feasible based on the single phototransistor neuron, which exempts the extra conversion components and circuits. After that, the same research group reported 3D monolithically integrated photoresponsive InGaAs biristor neurons over a synapse array for artificial visual perception, as presented in **Figure 16**a.[100] Such neuron can execute optical signal sensing, data collection, and conversion, as well

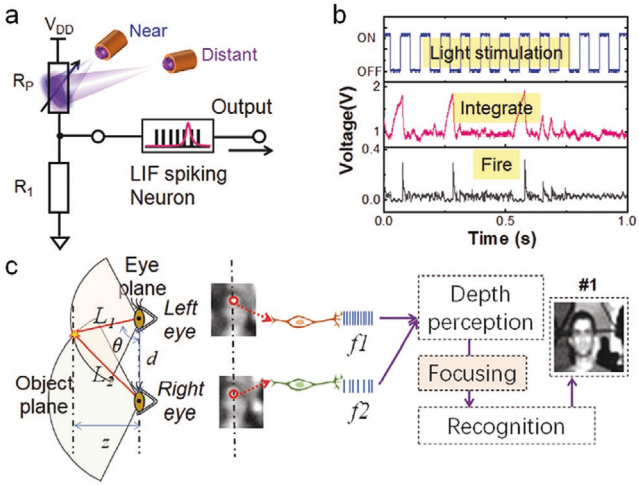

Figure 15. A photoelectric spiking neuron based on a photoresistor and a TaO_x memristive neuron. a) The circuit scheme of the photoelectric spiking neuron with near and distant light illumination. b) The encoded spikes of light stimuli based on the LIF model. c) A schematic image of the binocular positioning process in the human brain. Reproduced with permission.[98] Copyright 2022, Wiley-VCH GmbH.

© 2023 The Authors. Advanced Materials published by Wiley-VCH GmbH

15214095, 0, Downloaded from https://onlinelibrary.wiley.com/doi/10.1002/adma.202205047, Wiley Online Library on [19/06/2023]. See the Terms and Conditions (https://onlinelibrary.wiley.com/terms-and-conditions) on Wiley Online Library for rules of use; OA articles are governed by the applicable Creative Commons License

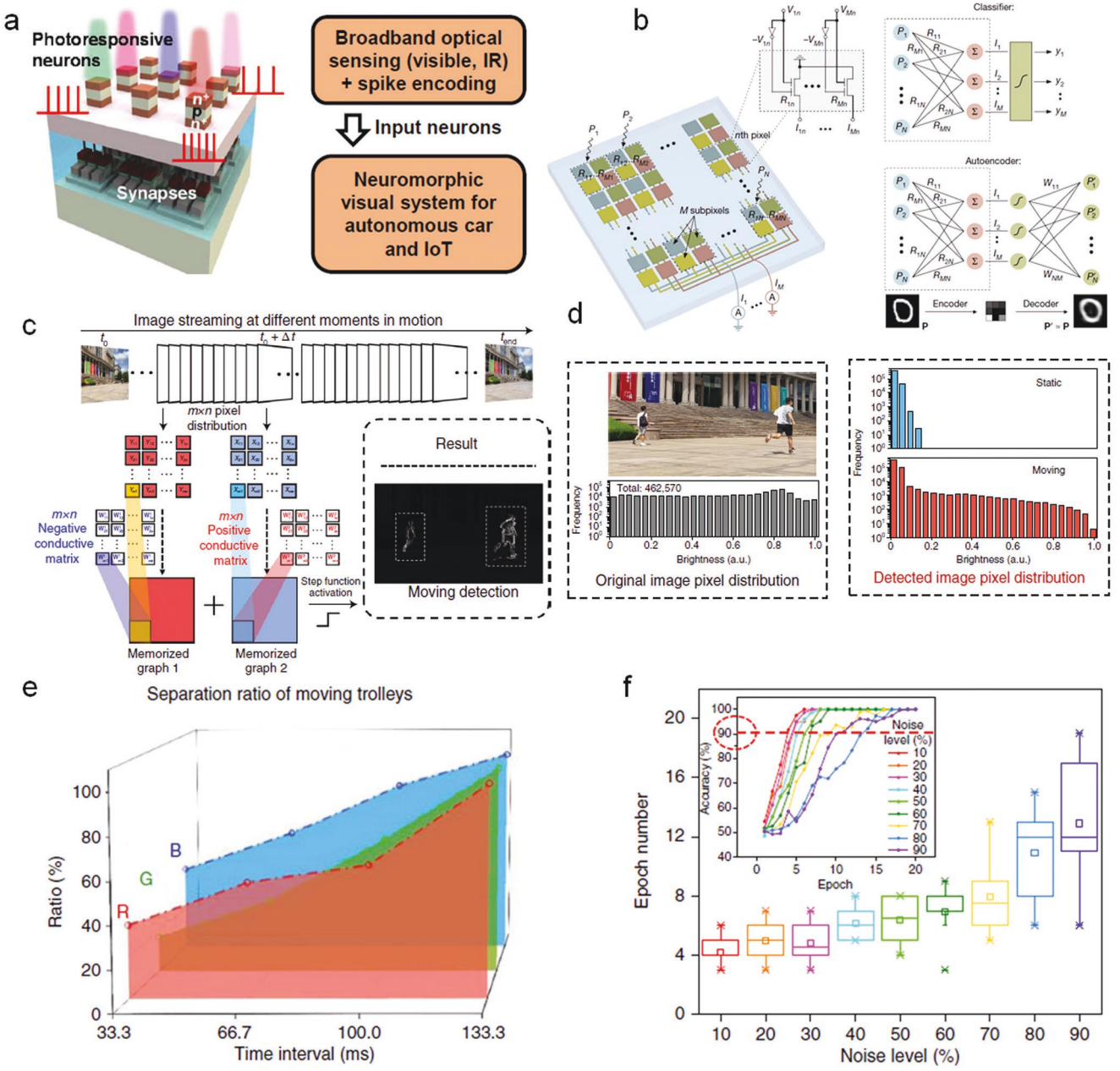

Figure 16. 2D-material-based visual neural networks and their applications. a) A schematic diagram of the 3D stackable neuromorphic visual system. Reproduced with permission.[100] Copyright 2021, IEEE. b) Schematics of the ANN imaging sensor array, classifier, and autoencoder. Reproduced with permission.[101] Copyright 2020, Springer Nature. c) The illustration of motion detection based on the 2D h-BN/WSe_2 retinomorphic hardware. d) The original image and its pixel brightness distribution; the pixel brightness distribution after motion detection with and without moving objects. e) Motion separation of red, green, and blue trolleys with various time intervals. f) The statistical distribution of the spent epoch number with trolley recognition accuracy above 90% for varying noise levels. Reproduced with permission.[102] Copyright 2020, Springer Nature.

as spiking signal transmission to a SNN simultaneously, enabling high efficiency and low energy budget. The 3D monolithic integration strategy shows promising potentials for future large-scale visual perception system with lower power consumption and higher integration density.

2D photosensitive materials are also employed to build visual neural networks. Mennel et al. demonstrated an ANN directly in an image sensor array.[101] Figure 16b shows the schematic diagram of the ANN. The image sensor consists of a photodiode array based on WSe_2. The photosensitivity of the diode, which represents the connection strength, can be modulated by the applied voltage, and thus the sensor array also functions as a neural network. Two neuromorphic functions, the classification and autoencoding, are successfully demonstrated. This computing in-sensor array can achieve image recognition in nanoseconds, learn the key features of an image, and reconstruct it with good fidelity. Zhou et al. reported a BP/Al_2O_3/WSe_2/h-BN heterostructure to implement all-in-one perception,

© 2023 The Authors. Advanced Materials published by Wiley-VCH GmbH

15214095, 0, Downloaded from https://onlinelibrary.wiley.com/doi/10.1002/adma.202205047, Wiley Online Library on [19/06/2023]. See the Terms and Conditions (https://onlinelibrary.wiley.com/terms-and-conditions) on Wiley Online Library for rules of use; OA articles are governed by the applicable Creative Commons License

memory, and computing for motion detection and recognition (MDR).[102] Figure 16c–f illustrates the retinomorphic hardware and corresponding MDR results. The photoresponse can be modulated either positively or negatively by optical stimuli, stored and differentially computed by the single device. The moving trichromatic trolleys are 100% successfully separated without ghosting. The detected image is then fed into a convolution neural network for further training. Fast and accurate (90%) trolley recognition is achieved in as few as four training epochs at 10% noise level. There are also a few other reports on the in-sensor computing systems based on 2D heterostructures for pattern recognition, classification, and so forth, suggesting that vdW materials may provide a promising platform for the neural network vision sensor.[94b,103]

Nevertheless, there are still some barriers impeding practical applications. First, the light absorption in thin 2D semiconductors is limited, which would make it difficult for low intensity light detection and pattern recognition. Second, the proposed design requires operation at a relatively large bias voltage, resulting in high power consumption. In addition, 2D materials often suffer from non-uniformity issues in large area growth, which adds to the challenges for large-scale integration. Besides, it would be beneficial if the photosensitive band of the sensing unit can be expanded to UV and IR spectrum to capture more information beyond human vision.

3.2. Skin Perceptual Neurons

Skin, as the largest organ, has many functionalities, for example, protection, sensing, and perception.[104] The critical demand on the emulation of human skin to endow the electronic skin system with higher intelligence has made the artificial tactile perception a popular research topic in recent years.[93b] Integration of sensing and processing units is a general methodology to emulate the behaviors of haptic sensory neuron. Haptic memory can easily be realized by combining pressure sensors and memristive devices. However, such a system cannot directly process the tactile patterns.[105] A spiking neuron that can encode and transmit the perceptual information is missing from simple sensor-memory systems.[106] In spite of their capability to differentiate tactile patterns, they lack the learning capabilities that are necessary for identification and recognition tasks.

To address this challenge, tactile perception learning process was successfully implemented by Zhang et al. using a haptic neuron system which comprises a piezoresistive sensor and a Nafion-based memristive neuron.[107] In the neuromorphic tactile processing system as illustrated in **Figure 17**a,b, spatiotemporally correlated stimuli can be integrated and modulated to enable parallel processing, and pattern recognition with high accuracy is achieved via repeated training.[108] Kim et al. demonstrated a tactile neuron and a perceptual neural network based on a semi-volatile carbon nanotube (CNT) transistor.[109] Figure 17c illustrates the design of the tactile sensor system. The system consists of a tactile sensor, a voltage-controlled oscillator circuit, one neuronal CNT transistor, and a synaptic CNT array, with the capability of identifying the temporally correlated stimuli and differentiating the features of tactile patterns. The recognition accuracy can be effectively improved with increased learning iterations.

In human skin, mechanonociceptors and thermal nociceptors are two major types of nociceptors. Yu et al. proposed a tactile perceptual neuron with both pressure decoding ability and nociceptive function, as illustrated in Figure 17d.[110] With a low power consumption, this tactile perceptual system can emulate acute and chronic pain, and nociceptive characteristics of allodynia and hyperalgesia in biological nociceptors. However, this artificial nociceptor is based on discrete sensors and not capable of producing spiking signals. To address this challenge, Zhu et al. recently reported an artificial mechanonociceptor array by integrating CNT-based pressure sensors with NbO_x memristors.[111] Key features of nociceptors under normal state and different levels of injuries are successfully demonstrated in the output neural spikes. There is also a study on thermal nociceptors based on diffusive memristors.[43a] The key functions of a nociceptor, such as no-adaptation and sensitization, have been demonstrated in a single device. Figure 17e,f shows bio-inspired artificial afferent nerves for tactile perceptual learning.[112] The two proposed artificial afferent nerves can achieve motion detection as well as handwriting recognition and classification. Notably, a hybrid bioelectronic reflex arc was constructed by combining the proposed artificial afferent nerve in Figure 17e with a biological efferent nerve to realize muscle motion control.[112a] These works show good promise for potential applications in neurorobotics and neuroprosthetics, and demonstrate promising strategies to realize an artificial tactile perceptual system.

3.3. Multisensory Neurons

Most of the previous research focused on the single-mode sensory perceptual system, which has not yet reached a level comparable to the integrated, multi-functional, and more efficient sensory perception in biological systems. Hence, it is of great significance to achieve the integration of multisensory information input or multisensory perception fusion in one hardware architecture. Wan et al. demonstrated a bimodal artificial sensory neuron with both visual and haptic perception.[113] Such a fused sensory perceptual system can collect optical and pressure information through photodetector and pressure sensor, respectively. **Figure 18**a shows the schematic illustration of the visual-haptic fused bimodal artificial sensory neuron. The motion control and recognition of multi-transparency alphabetic patterns are successfully demonstrated by such bimodal sensory neurons, as shown in Figure 18b,c. The good perceptual capability of this device can be attributed to the synergistic effect of visual and tactile feedback during the task. Recently, an artificial multisensory neuron with haptic-temperature fusion was reported based on a piezoresistive sensor and a VO_2 volatile memristor with intrinsic thermal sensitivity.[114] The schematic diagram of such multisensory perceptual system is shown in Figure 18d. By taking advantage of the coordination between haptic and temperature sensory inputs, the bimodal haptic-temperature fused sensory neuron can well achieve the recognition and classification of haptic/temperature patterns. This multisensory system is further developed by employing a

© 2023 The Authors. Advanced Materials published by Wiley-VCH GmbH

15214095, 0, Downloaded from https://onlinelibrary.wiley.com/doi/10.1002/adma.202205047, Wiley Online Library on [19/06/2023]. See the Terms and Conditions (https://onlinelibrary.wiley.com/terms-and-conditions) on Wiley Online Library for rules of use; OA articles are governed by the applicable Creative Commons License

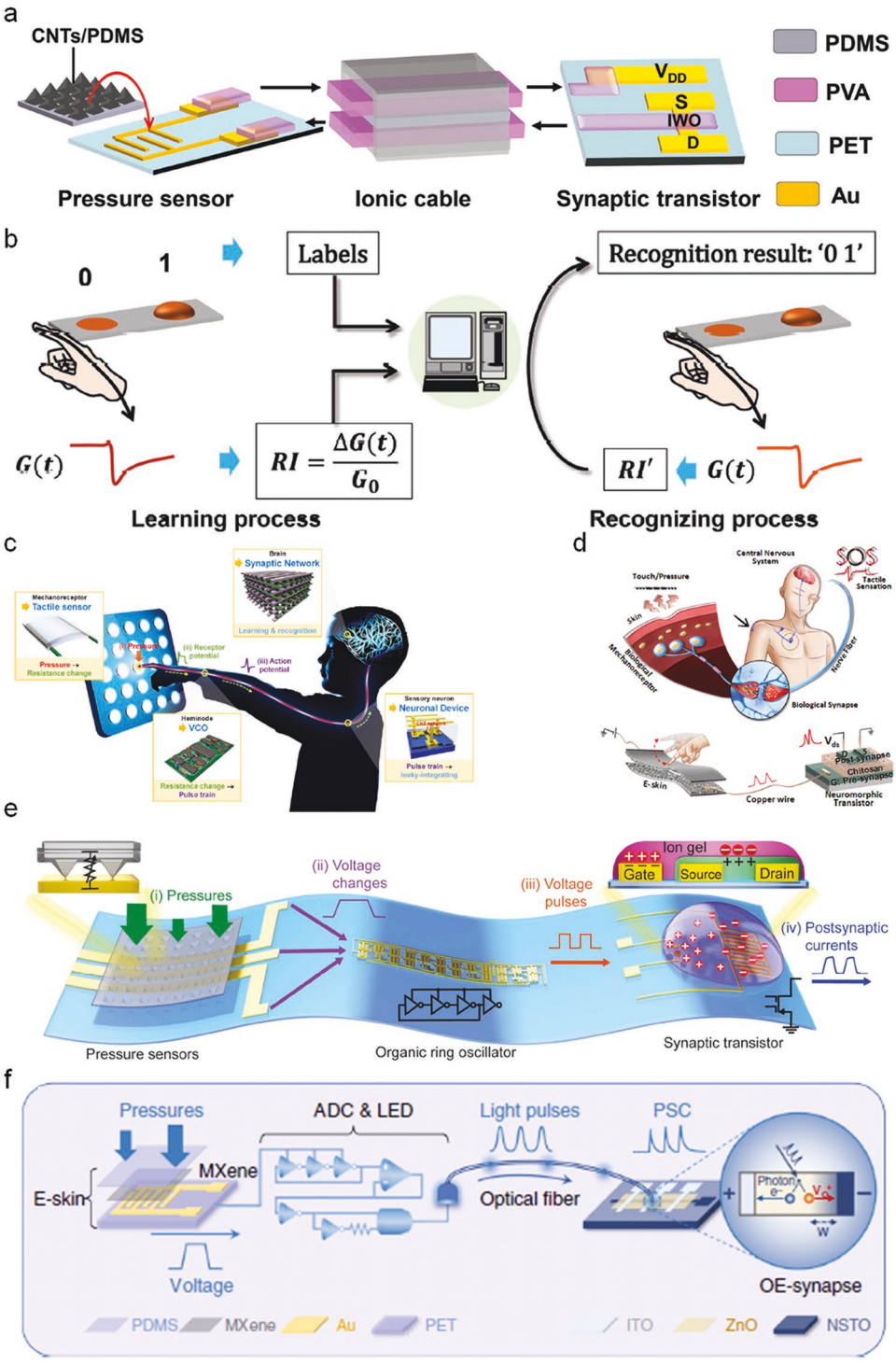

Figure 17. Artificial tactile perceptual neurons. a) An illustration of the CNT-based tactile perceptual neuron. b) A schematic diagram of the machine learning method for perceptual learning emulation. Reproduced with permission.[108] Copyright 2018, Wiley-VCH GmbH. c) Conceptual design of the proposed tactile neural system consisting of a tactile sensor device, a voltage-controlled oscillator, and a CNT transistor. Reproduced with permission.[109] Copyright 2020, Springer Nature. d) A schematic diagram of the human tactile afferent nerve and the proposed artificial tactile neural perceptual system. Reproduced with permission.[110] Copyright 2020, American Chemical Society. e) A schematic illustration of the flexible organic artificial afferent nerve. Reproduced with permission.[112a] Copyright 2018, the American Association for the Advancement of Science. f) A schematic diagram of the artificial optoelectronic spiking afferent nerves. Reproduced with permission.[112b] Copyright 2020, Springer Nature.

© 2023 The Authors. Advanced Materials published by Wiley-VCH GmbH

15214095, 0, Downloaded from https://onlinelibrary.wiley.com/doi/10.1002/adma.202205047, Wiley Online Library on [19/06/2023]. See the Terms and Conditions (https://onlinelibrary.wiley.com/terms-and-conditions) on Wiley Online Library for rules of use; OA articles are governed by the applicable Creative Commons License

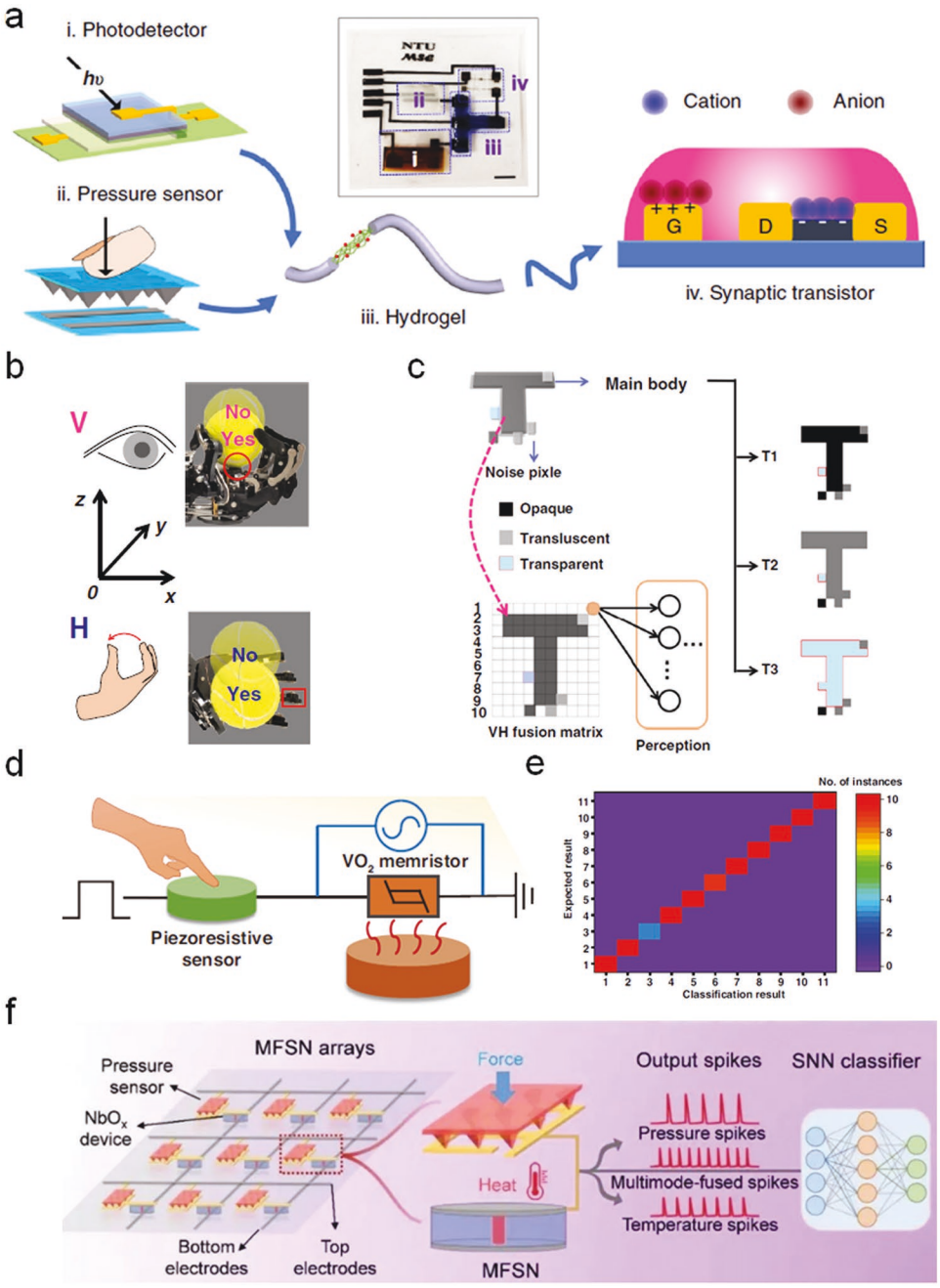

Figure 18. Multisensory neurons. a) A schematic illustration of the visual-haptic fused bimodal artificial sensory neuron. The illustration of b) motion control and c) multi-transparency pattern recognition task based on the bimodal artificial sensory neuron. Reproduced with permission.[113] Copyright 2020, Springer Nature. d) A schematic diagram of a multisensory perceptual system with haptic-temperature fusion. e) The confusion matrix of the classification testing results. Reproduced under the terms of the CC-BY license.[114] Copyright 2022, the Authors. Published by Wiley-VCH GmbH. f) A schematic diagram of the multimode-fused spiking neuron array and the SNN classifier. Reproduced with permission.[116] Copyright 2022, Wiley-VCH GmbH.

scaling resistor to adapt the high quality epitaxial VO_2 neuron to sensors with different resistance level.[115] The sensation and encoding of illuminance, temperature, pressure, and curvature signals are demonstrated using this multisensory neuron.

Most of the abovementioned works are at single-device level and their function of multi-modal perception fusion is often achieved at the expense of each individual sensing mode performance. As a system-level implementation, Zhu et al. demonstrated a pressure and temperature multimode-fused spiking neuron system by heterogeneously integrating pressure sensors and NbO_x memristors into an array, as shown in Figure 18f.[116] The pressure and temperature information can be not only fused into one spike train, but also distinguished by decoupling the spike frequency and amplitude. This ensures that the system has a strong capability to distinguish and perceive different external stimuli while having good data compression and

© 2023 The Authors. Advanced Materials published by Wiley-VCH GmbH

15214095, 0, Downloaded from https://onlinelibrary.wiley.com/doi/10.1002/adma.202205047, Wiley Online Library on [19/06/2023]. See the Terms and Conditions (https://onlinelibrary.wiley.com/terms-and-conditions) on Wiley Online Library for rules of use; OA articles are governed by the applicable Creative Commons License

15214095, 0, Downloaded from https://onlinelibrary.wiley.com/doi/10.1002/adma.202205047, Wiley Online Library on [19/06/2023]. See the Terms and Conditions (https://onlinelibrary.wiley.com/terms-and-conditions) on Wiley Online Library for rules of use; OA articles are governed by the applicable Creative Commons License

conversion capabilities. Such multisensory neuron systems can mimic the human perception system toward more compact, more functional, and more efficient intelligent systems. There are also critical demands on artificial auditory, olfactory, and other sensory neurons emulation to achieve the full hardware implementation of human sensory perceptual system. An artificial gustatory neuron has been reported recently.[117] However, relevant reports remain rare so far.

4. Challenges and Perspectives

In the past a few years, artificial neuronal devices based on diverse volatile switching materials have captured a broad range of neuronal dynamics which are further exploited to implement various ANN architectures. However, there is still a significant gap between the demonstrated NC systems and those needed for practical large scale computing applications. A series of barriers remain to be overcome toward approaching the level of sophistication of their biological counterparts. The challenges for further research in this field mainly exist in three aspects, individual device performance, system-level computing capability, and ANN architecture innovation.

Further improvements of individual neuronal device parameters are required by more powerful and energy efficient NC systems. Neuroscience research shows that the total energy cost of biological neurons generating a single action potential and passing it though the axon is around tens to hundreds of femtojoule, and the power consumption of a neuron in the resting state is at picowatt level.[16,86b,118] By contrast, the power consumption of neuronal oscillators input voltage can exceed microwatt even when they are driven by a subthreshold input and do not fire neural spikes at all.[8a,11d,119] The energy cost is even higher when resistive switching occurs, as shown in Table 2. Depending on the switching mechanism, some possible strategies can be used to address this problem. Changing the geometric parameters of the IMT oscillators, for example, employing nanowires[17b,25b,120] or atomically thin films[39] as the channel, can effectively reduce the device conductance. Similarly, minimizing the area of switching media in vertical non-filamentary memristors can also reduce the operating current. Topological insulators that can generate spin-transfer torque may have the potential to replace the ferromagnetic layers in MTJ devices and improve the energy efficiency.[121] As to LIF neurons, the energy consumption in the resting state can be suppressed by employing switching materials with a high on/off ratio. In this case, the resistive switching and relaxation process dominates the energy consumption. Similar to the situation of non-volatile memory, the switching energy can be decreased by reducing the effective thickness of switching media in memristors,[122] or the volume of active phase transition region in PCM neurons.[10c,123] Meanwhile, attempts to reduce energy consumption should also take the working frequency into consideration, since the lower operating current tends to slow down the switching speed. Some LIF neurons based on ECM or electrolyte-gated FET are reported to work at low frequency. Introducing mobile ions to these devices via doping or oxidation may help address the problem.[124]

In terms of reliability and reproducibility, the cycle-to-cycle variation in individual device operation and device-to-device variation in batch fabrication are commonly regarded as problems of memory devices; however, as we mentioned, they can be employed to mimic neuronal functions such as probabilistic firing and PPC in a NC system.[10a] The key point is how to obtain a robust stochastic activation function for individual devices and a more reproducible distribution of neuronal response among a device group. Inspired by the report of controlling grain boundaries in MoS_2 synthesis,[125] one possible solution is to intentionally create active sites that favor filament formation or phase transition during device fabrication, so that the switching would prefer to occur at these sites in a more consistent manner. Another problem in exploiting the stochasticity of neuronal oscillators is the small voltage range of their stochastic oscillation regime, typically within tens to hundreds of millivolt, which makes the device operation vulnerable to noise.[17b,39] Increasing the series resistance in the oscillatory circuit can broaden the operation regime but it would also require a higher operating voltage. A reconfigurable stochastic neuron with dynamically tunable series resistance may provide a possible solution to this problem.[26a] MTJ neurons also have the noise tolerance issue because they suffer from low on/off ratio, which makes recognizing and counting their neural spikes difficult in a noisy context. Novel designs of MTJ memory cells with more auxiliary components can enhance the on/off ratio at the expense of compactness. For example, Patel et al. showed that a 2T1R cell possesses over five times higher on/off ratio than a traditional 1T1R cell.[126]

The system-level hardware implementation of NC systems centered with artificial neuronal devices focuses on utilizing certain neuronal dynamics, such as neuronal coupling, LIF behavior, or stochastic activation, to demonstrate novel ANN architectures and solve computational problems that are particularly suitable for these ANNs, as we summarize in Table 1. These works, on one side, are very encouraging since they confirm that even only mimicking a small fraction of biological neuronal dynamics can provide considerable computing capability. On the other side, these demonstrations remain rudimentary. Each demonstrated ANN is typically dedicated to solving a specific type of problems with a small input size. Some theoretical and engineering challenges need to be overcome before fully realizing the computing power of these ANN architectures. ONNs were originally proposed to be able to solve general computational problems since they permit the realization of Boolean logic operations.[127] However, the reformulation of general problems that are conventionally solved by level-based circuits using the frequency or phase state of neuronal oscillators remains challenging. The demonstrations we described in Section 2.1.3 serve as good reference in this regard. On top of them, some simulation works may provide useful guide. For example, Hoppensteadt and Izhikevich set the mathematical basis about applying Hebbian learning rules to an ONN by imposing dynamic connectivity via external input.[128] Follmann et al.,[129] Yogen et al.,[55a] and Popescu et al.[130] conceive different coupling schemes of MTJ neurons for executing pattern recognition. Shukla et al.[60] and Csaba et al.[51,52] show how to use IMT oscillators to perform image processing and pattern recognition, respectively. A recent simulation work provides a detailed tutorial about how to control the coupling

© 2023 The Authors. Advanced Materials published by Wiley-VCH GmbH

state of IMT neuronal oscillators via subharmonic injection locking.[131] Furthermore, one major bottleneck that prevents ONN hardware from practical application is the difficulty of realizing full coupling between neurons.[51] The number of required interconnects increases quadratically as the number of neurons increases, and would become overwhelming quickly as the problem size goes big. Therefore, a vertical integrated structure that arranges neuronal oscillators and interconnection wires in different planes is needed. Strategies to realize partial interconnection via a global microwave current or magnetic field have been introduced in Section 2.1.3. As for the coupling mode, besides the two extremes, resistive and capacitive, Raychowdhury et al.[54a] proposed that a bistable mode, which means both the in-phase and antiphase locking modes are stable, can be realized by properly tuning the coupling conductance and capacitance. Assisted by the stochasticity of neuronal oscillators, the bistable mode may act as an intermediate state between two extremes and potentially provides a binary degree of freedom in ONNs, but its applicability needs further experimental confirmation.

Different from ONNs, SNNs are dedicated to applications like pattern recognition and classification.[132] As mentioned before, existing SNN hardware has managed to demonstrate both supervised[24a] and unsupervised learning[24b,c] for image recognition using simplified Hebbian rules and gradient descent methods. However, all these SNNs have only a single layer of fewer than ten neurons. Therefore, they can only process very small pixel images and execute simple classification jobs. SNNs that consist of over hundreds of neurons should be implemented to reach the computing power required by more practical applications. Moreover, the hardware implementation of multilayer SNNs based on volatile switching devices has not been realized. One engineering challenge is the coordination between neuronal and synaptic devices in terms of fabrication compatibility, operating voltage (current) level, and available dynamics (plasticity). Memristive neural networks have shown advantages in this term since memristors can serve as both neurons and synapses without complicated auxiliary circu its.[7d,18c,24a,68b] Other devices with both volatile and non-volatile features like PCM, FeFETs, and spintronic devices are also good candidates, given their relatively mature fabrication techniques.[133] Another critical problem comes from the heterogeneity of input and output neural spikes of neuronal devices. Both the amplitude and morphology of output neural spike trains are usually very different from those of input ones for single neurons.[13c,42a,69b,73c,87] Therefore, the output of a neuron cannot be directly fed to the next one, which severely obstructs the operation of multilayer SNNs. Besides, synaptic devices and wires may also induce significant input voltage loss over the course of signal transport.[15a] Therefore, auxiliary circuits that compensate voltage loss and rectify pulse morphology should be added to the synaptic nodes in multilayer SNNs. In terms of learning rules, given that the discontinuous nature of SNNs prevents the application of traditional gradient-based methods, other learning rules such as SpikeProp algorithm,[134] Theta-learning rules,[135] backpropagation through time,[136] and three factor learning rules[137] may be applied to multilayer SNNs.[138]

The reports of BMs[26] and BNs[27] are good initial attempts to take advantage of neuronal stochasticity in ANNs. However, the functionality of BNs is only demonstrated via simulation, with the device parameters extracted from experiments. The physical construction of such BNs should be the next step. As we mentioned before, a hardware scheme of BN based on stochastic neurons and peripheral circuitries have been proposed.[27b] Though BM has been experimentally realized using a few neurons controlled by a field programmable gate array board or a microcontroller, the demonstrated optimization problem in this work is either so simple that in most cases the system energy drops monotonically after every iteration,[26a] or too small in size compared with practical needs.[26b] More efforts toward solving a more general problem with a larger size are expected in the future demonstration of stochastic ANNs to better show their computing efficacy.

To bridge the gap between ANNs and biological neural networks, one possible strategy is to develop innovative architectures that exploit more advanced neuronal dynamics. The interaction between neurons plays a critical role in the operation of biological neural networks. A neuronal assembly, defined as a group of neurons with strong mutual excitatory connections, is the biological basis of short term and long term memory.[132] Synchronization of firing times can be easily realized by coupling groups of neuron oscillators in ONNs; however, it remains challenging to realize synchronization among spiking neurons and construct assembly code in SNNs.[139] The research on neuronal interaction can start from realizing self-coupling of a single neuron or the coupling between a few neurons. For example, Zhang et al. designed a memristive autapse connected to a neuron to enhance neuronal firing rate and spiking modulation capability.[140] Moujahid et al. indicate that HH neurons coupled by electrical synapses show the best information transmission performance at a low energy cost.[86a] Advances have been made toward realizing the synchronization of the firing activity of multiple neurons to form temporal correlation between events and local self-clocking,[24b,38] including mimicking neural synchrony using stochastic plasticity[141] and the hardware demonstration of spatial-temporal code.[142] Besides, neuroscience and computer science research on this topic may provide some inspirations. For example, Hopfield and Brody proposed transient synchrony as a collective mechanism for spatiotemporal integration and indicated that the event of collective synchronization of specific groups of neurons in response to a given stimulus may constitute a basic network-level building block.[143] Furthermore, the incorporation of inhibitory neurons to current ANNs is supposed to be necessary because they perform many important functions in biological nervous system such as mediating lateral competition, forming negative feedback loops as distributed clocks, and enabling spatiotemporal coordination.[7a] Lateral inhibition has been deployed in many fully connected feedforward networks to enhance the input discrimination and improve energy efficiency.[24a,144] However, the inhibition operation in these works are fulfilled by software or CMOS components instead of inhibitory neurons. Neuronal inhibition has been captured by neuronal devices based on a single MOSFET[145] or a FeFET circuit,[13a] but the reports on inhibitory neurons remain very rare. The research on involving inhibition dynamics and modeling their functionality in ANNs is not only an interesting challenge for the NC community, but also beneficial to computer science and neuroscience research.[146] In addition, considering that a great diversity of neurons collaborate together for the function of biological nervous systems,[147] hierarchical control structures dedicated to

© 2023 The Authors. Advanced Materials published by Wiley-VCH GmbH

15214095, 0, Downloaded from https://onlinelibrary.wiley.com/doi/10.1002/adma.202205047, Wiley Online Library on [19/06/2023]. See the Terms and Conditions (https://onlinelibrary.wiley.com/terms-and-conditions) on Wiley Online Library for rules of use; OA articles are governed by the applicable Creative Commons License

regulating the information flow in biological neural networks, such as neurons in spinal cord and thalamus should have their counterparts in more advanced ANNs.[148]

Despite the significant progress, the artificial sensory neuron system is still in its infancy. For more inspiration toward the next development stage, a more comprehensive and in-depth understanding of the biological behaviors and patterns of sensory neurons would be beneficial for the construction of artificial sensory neuron systems.[149] At the individual device level, flexible sensory neurons with multidimensional perceptual fusion and processing capability are highly desired.[150] Emerging materials, for example, organic semiconductors, which are flexible and applicable to large-area manufacturing, hold great potential for future intelligent sensory neuron applications.[151] More neuronal dynamics, such as stochastic resonance and coherence resonance, can be employed to enhance signal detection.[152] Additionally, device/algorithm co-design may provide new opportunities to optimize the operating speed and power efficiency. Furthermore, miniaturization of neuronal devices and their related periphery circuits without the loss of multi-functionality is essential for integrated artificial perceptual neuron systems with higher complexity. System-level integration is challenging for such systems with many functional components and modules, including sensors, memory, and processing units, as well as peripheral circuits.[93b] The compatibility of different components in terms of electric and mechanical properties, as well as performance-power consumption trade-off, needs to be taken into consideration. A standard or optimized fabrication workflow is extremely desirable to not only overcome the compatibility problem but also enable higher scalability and reliability.[93a] Besides, artificial nervous systems that resemble the biological nervous system hierarchy, which involves the communication and collaboration between peripheral and central nervous systems, have yet to be implemented. An initial demonstration that combines the function of artificial sensory and cortical neurons can be a good starting point.

To sum up, many challenges exist in building more powerful artificial neuronal devices and neural networks. They originate from the challenges in material selection, device fabrication, circuit operation, and more importantly, the diversity of neuron types and the remaining knowledge gaps regarding the organization of computations in biological nervous systems.[153] Despite these difficulties, implementing the key aspects of typical neurons and neural circuits would yield a deeper understanding of biological systems and shed light on developing more practical artificial intelligent systems.

Acknowledgements

H.L., H.C., J.W., J.M., Z.D., N.W., and H.W. acknowledge the support in part from Army Research Office (grant no. W911NF1810268) and National Science Foundation (grant no. CMMI-2240407). Y.Q. and Y.Z. acknowledge National Science Foundation (grant no. ECCS-2045001). J.Z., S.L., and X.Z. acknowledge the support from the Pennsylvania Infrastructure Technology Alliance (PITA) program.

Conflict of Interest

The authors declare no conflict of interest.

Keywords

artificial neurons, brain emulation, neuromorphic computing, sensory neurons, spiking neural networks

Received: June 3, 2022
Revised: December 2, 2022
Published online:

[1] P. A. Merolla, J. V. Arthur, R. Alvarez-Icaza, A. S. Cassidy, J. Sawada, F. Akopyan, B. L. Jackson, N. Imam, C. Guo, Y. Nakamura, *Science* **2014**, *345*, 668.

[2] a) J.-s. Seo, B. Brezzo, Y. Liu, B. D. Parker, S. K. Esser, R. K. Montoye, B. Rajendran, J. A. Tierno, L. Chang, D. S. Modha, presented at 2011 IEEE Custom Integrated Circuits Conf. (CICC), San Jose, CA, USA, September **2011**; b) I. Sourikopoulos, S. Hedayat, C. Loyez, F. Danneville, V. Hoel, E. Mercier, A. Cappy, *Front Neurosci.* **2017**, *11*, 123.

[3] a) J. Zhu, T. Zhang, Y. Yang, R. Huang, *Appl. Phys. Rev.* **2020**, *7*, 011312; b) G. Lee, J. H. Baek, F. Ren, S. J. Pearton, G. H. Lee, J. Kim, *Small* **2021**, *17*, 2100640.

[4] a) D. B. Strukov, G. S. Snider, D. R. Stewart, R. S. Williams, *Nature* **2008**, *453*, 80; b) S. H. Jo, T. Chang, I. Ebong, B. B. Bhadviya, P. Mazumder, W. Lu, *Nano Lett.* **2010**, *10*, 1297.

[5] a) M. Suri, O. Bichler, D. Querlioz, O. Cueto, L. Perniola, V. Sousa, D. Vuillaume, C. Gamrat, B. DeSalvo, presented at 2011 Int. Electron Devices Meeting, Washington, DC, USA, December **2011**; b) M. Suri, O. Bichler, D. Querlioz, B. Traoré, O. Cueto, L. Perniola, V. Sousa, D. Vuillaume, C. Gamrat, B. DeSalvo, *J. Appl. Phys.* **2012**, *112*, 054904.

[6] A. F. Vincent, J. Larroque, N. Locatelli, N. B. Romdhane, O. Bichler, C. Gamrat, W. S. Zhao, J.-O. Klein, S. Galdin-Retailleau, D. Querlioz, *IEEE Trans. Biomed. Circuits Syst.* **2015**, *9*, 166.

[7] a) J. Tang, F. Yuan, X. Shen, Z. Wang, M. Rao, Y. He, Y. Sun, X. Li, W. Zhang, Y. Li, *Adv. Mater.* **2019**, *31*, 1902761; b) M. A. Zidan, Y. Jeong, J. Lee, B. Chen, S. Huang, M. J. Kushner, W. D. Lu, *Nat. Electron.* **2018**, *1*, 411; c) F. M. Bayat, M. Prezioso, B. Chakrabarti, H. Nili, I. Kataeva, D. Strukov, *Nat. Commun.* **2018**, *9*, 2331; d) P. Yao, H. Wu, B. Gao, J. Tang, Q. Zhang, W. Zhang, J. J. Yang, H. Qian, *Nature* **2020**, *577*, 641.

[8] a) M. D. Pickett, G. Medeiros-Ribeiro, R. S. Williams, *Nat. Mater.* **2013**, *12*, 114; b) L. Gao, P.-Y. Chen, S. Yu, *Appl. Phys. Lett.* **2017**, *111*, 103503; c) K. Moon, E. Cha, J. Park, S. Gi, M. Chu, K. Baek, B. Lee, S. Oh, H. Hwang, presented at 2015 IEEE Int. Electron Devices Meeting (IEDM), Washington, DC, USA, December **2015**.

[9] a) T. C. Jackson, A. A. Sharma, J. A. Bain, J. A. Weldon, L. Pileggi, *IEEE J Emerging Sel. Top. Circuits Syst.* **2015**, *5*, 230; b) A. A. Sharma, Y. Li, M. Skowronski, J. A. Bain, J. A. Weldon, *IEEE Trans. Electron Devices* **2015**, *62*, 3857; c) Z. Wang, S. Joshi, S. E. Savel'ev, H. Jiang, R. Midya, P. Lin, M. Hu, N. Ge, J. P. Strachan, Z. Li, *Nat. Mater.* **2017**, *16*, 101.

[10] a) T. Tuma, A. Pantazi, M. L. Gallo, A. Sebastian, E. Eleftheriou, *Nat. Nanotechnol.* **2016**, *11*, 693; b) I. Chakraborty, G. Saha, A. Sengupta, K. Roy, *Sci. Rep.* **2018**, *8*, 12980; c) C. D. Wright, P. Hosseini, J. A. V. Diosdado, *Adv. Funct. Mater.* **2013**, *23*, 2248.

[11] a) M. Sharad, C. Augustine, G. Panagopoulos, K. Roy, presented at 2012 IEEE/ACM Int. Symp. on Nanoscale Architectures (NANOARCH), Amsterdam, Netherlands, July **2012**; b) M. Sharad, D. Fan, K. Roy, *J. Appl. Phys.* **2013**, *114*, 234906; c) A. Sengupta, S. H. Choday, Y. Kim, K. Roy, *Appl. Phys. Lett.* **2015**, *106*, 143701; d) J. Torrejon, M. Riou, F. A. Araujo, S. Tsunegi, G. Khalsa, D. Querlioz, P. Bortolotti, V. Cros, K. Yakushiji, A. Fukushima, *Nature* **2017**, *547*, 428.

© 2023 The Authors. Advanced Materials published by Wiley-VCH GmbH

15214095, 0, Downloaded from https://onlinelibrary.wiley.com/doi/10.1002/adma.202205047, Wiley Online Library on [19/06/2023]. See the Terms and Conditions (https://onlinelibrary.wiley.com/terms-and-conditions) on Wiley Online Library for rules of use; OA articles are governed by the applicable Creative Commons License

[12] a) S. Li, W. Kang, Y. Huang, X. Zhang, Y. Zhou, W. Zhao, *Nanotechnology* **2017**, *28*, 31LT01; b) X. Chen, W. Kang, D. Zhu, X. Zhang, N. Lei, Y. Zhang, Y. Zhou, W. Zhao, *Nanoscale* **2018**, *10*, 6139; c) X. Liang, X. Zhang, J. Xia, M. Ezawa, Y. Zhao, G. Zhao, Y. Zhou, *Appl. Phys. Lett.* **2020**, *116*, 122402; d) N. Bindal, C. A. C. Ian, W. S. Lew, B. K. Kaushik, *Nanotechnology* **2021**, *32*, 215204.

[13] a) Z. Wang, B. Crafton, J. Gomez, R. Xu, A. Luo, Z. Krivokapic, L. Martin, S. Datta, A. Raychowdhury, A. I. Khan, presented at 2018 IEEE Int. Electron Devices Meeting (IEDM), San Francisco, CA, USA, December **2018**; b) H. Mulaosmanovic, E. Chicca, M. Bertele, T. Mikolajick, S. Slesazeck, *Nanoscale* **2018**, *10*, 21755; c) C. Chen, M. Yang, S. Liu, T. Liu, K. Zhu, Y. Zhao, H. Wang, Q. Huang, R. Huang, presented at 2019 Symp. on VLSI Technology, Tokyo, Japan, June **2019**.

[14] E. Toomey, K. Segall, M. Castellani, M. Colangelo, N. Lynch, K. K. Berggren, *Nano Lett.* **2020**, *20*, 8059.

[15] a) S. Choi, J. Yang, G. Wang, *Adv. Mater.* **2020**, *32*, 2004659; b) H. Bian, Y. Y. Goh, Y. Liu, H. Ling, L. Xie, X. Liu, *Adv. Mater.* **2021**, *33*, 2006469.

[16] D. Purves, G. J. Augustine, D. Fitzpatrick, W. Hall, A.-S. LaMantia, L. White, *Neurosciences*, De Boeck Supérieur, Louvain-la-Neuve **2019**.

[17] a) A. Sengupta, P. Panda, P. Wijesinghe, Y. Kim, K. Roy, *Sci. Rep.* **2016**, *6*, 30039; b) M. Jerry, A. Parihar, B. Grisafe, A. Raychowdhury, S. Datta, presented at 2017 Symp. on VLSI Technology, Kyoto, Japan, June **2017**; c) S. Kumar, J. P. Strachan, R. S. Williams, *Nature* **2017**, *548*, 318.

[18] a) D. S. Jeong, C. S. Hwang, *Adv. Mater.* **2018**, *30*, 1704729; b) C.-H. Kim, S. Lim, S. Y. Woo, W.-M. Kang, Y.-T. Seo, S.-T. Lee, S. Lee, D. Kwon, S. Oh, Y. Noh, *Nanotechnology* **2018**, *30*, 032001; c) H.-M. Huang, Z. Wang, T. Wang, Y. Xiao, X. Guo, *Adv. Intell. Syst.* **2020**, *2*, 2000149.

[19] a) M. F. Bear, B. W. Connors, M. A. Paradiso, *Neuroscience*, Vol. *2*, Lippincott Williams & Wilkins, Philadelphia **2007**; b) E. R. Kandel, J. H. Schwartz, T. M. Jessell, D. o. Biochemistry, M. B. T. Jessell, S. Siegelbaum, A. Hudspeth, *Principles of Neural Science*, Vol. *4*, McGraw-Hill, New York **2000**.

[20] a) E. T. Rolls, G. Deco, *The Noisy Brain: Stochastic Dynamics as a Principle of Brain Function*, Vol. *34*, Oxford University Press, Oxford **2010**; b) G. Deco, E. T. Rolls, R. Romo, *Prog. Neurobiol.* **2009**, *88*, 1.

[21] a) J. J. Hopfield, *Proc. Natl. Acad. Sci. U. S. A.* **1982**, *79*, 2554; b) W. Maass, *Neural Networks* **1997**, *10*, 1659; c) R. Zand, K. Y. Camsari, S. D. Pyle, I. Ahmed, C. H. Kim, R. F. DeMara, presented at Proceedings of the 2018 on Great Lakes Symp. on VLSI, Chicago, IL, USA, May **2018**.

[22] E. Schneidman, I. Segev, N. Tishby, presented at Advances in Neural Information Processing Systems, Denver, CO, USA, December **2000**.

[23] A. H. Zhang, G. Sharma, E. A. Undheim, X. Jia, M. Mobli, *Neurosci. Lett.* **2018**, *679*, 35.

[24] a) Z. Wang, S. Joshi, S. Savel'ev, W. Song, R. Midya, Y. Li, M. Rao, P. Yan, S. Asapu, Y. Zhuo, H. Jiang, P. Lin, C. Li, J. H. Yoon, N. K. Upadhyay, J. Zhang, M. Hu, J. P. Strachan, M. Barnell, Q. Wu, H. Wu, R. S. Williams, Q. Xia, J. J. Yang, *Nat. Electron.* **2018**, *1*, 137; b) Q. Duan, Z. Jing, X. Zou, Y. Wang, K. Yang, T. Zhang, S. Wu, R. Huang, Y. Yang, *Nat. Commun.* **2020**, *11*, 3399; c) X. Li, J. Tang, Q. Zhang, B. Gao, J. J. Yang, S. Song, W. Wu, W. Zhang, P. Yao, N. Deng, *Nat. Nanotechnol.* **2020**, *15*, 776.

[25] a) A. Parihar, N. Shukla, M. Jerry, S. Datta, A. Raychowdhury, *Sci. Rep.* **2017**, *7*, 911; b) S. Dutta, A. Khanna, A. Assoa, H. Paik, D. Schlom, Z. Toroczkai, A. Raychowdhury, S. Datta, *Nat. Electron.* **2021**, *4*, 502; c) S. Dutta, A. Parihar, A. Khanna, J. Gomez, W. Chakraborty, M. Jerry, B. Grisafe, A. Raychowdhury, S. Datta, *Nat. Commun.* **2019**, *10*, 3299.

[26] a) X. Yan, J. Ma, T. Wu, A. Zhang, J. Wu, M. Chin, Z. Zhang, M. Dubey, W. Wu, M. S.-W. Chen, *Nat. Commun.* **2021**, *12*, 5710; b) W. A. Borders, A. Z. Pervaiz, S. Fukami, K. Y. Camsari, H. Ohno, S. Datta, *Nature* **2019**, *573*, 390.

[27] a) P. Debashis, V. Ostwal, R. Faria, S. Datta, J. Appenzeller, Z. Chen, *Sci. Rep.* **2020**, *10*, 16002; b) S. Choi, G. S. Kim, J. Yang, H. Cho, C. Y. Kang, G. Wang, *Adv. Mater.* **2022**, *34*, 2104598.

[28] a) B. Lalevic, M. Shoga, *Thin Solid Films* **1981**, *75*, 199; b) S. Kumar, Z. Wang, N. Davila, N. Kumari, K. J. Norris, X. Huang, J. P. Strachan, D. Vine, A. Kilcoyne, Y. Nishi, *Nat. Commun.* **2017**, *8*, 658.

[29] Y. Taketa, F. Kato, M. Nitta, M. Haradome, *Appl. Phys. Lett.* **1975**, *27*, 212.

[30] G. Liu, B. Debnath, T. R. Pope, T. T. Salguero, R. K. Lake, A. A. Balandin, *Nat. Nanotechnol.* **2016**, *11*, 845.

[31] J. Wang, S. Hu, X. Zhan, Q. Yu, Z. Liu, T. P. Chen, Y. Yin, S. Hosaka, Y. Liu, *Sci. Rep.* **2018**, *8*, 12546.

[32] a) S. Lashkare, S. Chouhan, T. Chavan, A. Bhat, P. Kumbhare, U. Ganguly, *IEEE Electron Device Lett.* **2018**, *39*, 484; b) S. Lashkare, P. Kumbhare, V. Saraswat, U. Ganguly, *IEEE Electron Device Lett.* **2018**, *39*, 1437.

[33] Y. Yang, H. Li, *Adv. Electron. Mater.* **2022**, *8*, 2200094.

[34] M. Lee, S. W. Cho, S. J. Kim, J. Y. Kwak, H. Ju, Y. Yi, B.-k. Cheong, S. Lee, *Phys. Rev. Appl.* **2020**, *13*, 064056.

[35] Z. Wang, S. Khandelwal, A. I. Khan, *IEEE Electron Device Lett.* **2017**, *38*, 1614.

[36] a) R. Khymyn, I. Lisenkov, J. Voorheis, O. Sulymenko, O. Prokopenko, V. Tiberkevich, J. Akerman, A. Slavin, *Sci. Rep.* **2018**, *8*, 15727; b) P. Villard, U. Ebels, D. Houssameddine, J. Katine, D. Mauri, B. Delaet, P. Vincent, M.-C. Cyrille, B. Viala, J.-P. Michel, *IEEE J. Solid-State Circuits* **2009**, *45*, 214.

[37] X. Zhang, Y. Zhuo, Q. Luo, Z. Wu, R. Midya, Z. Wang, W. Song, R. Wang, N. K. Upadhyay, Y. Fang, *Nat. Commun.* **2020**, *11*, 51.

[38] G. Kim, J. H. In, Y. S. Kim, H. Rhee, W. Park, H. Song, J. Park, K. M. Kim, *Nat. Commun.* **2021**, *12*, 2906.

[39] H. Liu, T. Wu, X. Yan, J. Wu, N. Wang, Z. Du, H. Yang, B. Chen, Z. Zhang, F. Liu, *Nano Lett.* **2021**, *21*, 3465.

[40] Y. Yu, B. Zhao, J. M. Goodwill, Y. Ma, J. A. Bain, M. Skowronski, *ACS Appl. Electron. Mater.* **2020**, *2*, 683.

[41] H. Lin, C. Wang, Q. Deng, C. Xu, Z. Deng, C. Zhou, *Nonlinear Dyn.* **2021**, *106*, 959.

[42] a) P. Stoliar, J. Tranchant, B. Corraze, E. Janod, M. P. Besland, F. Tesler, M. Rozenberg, L. Cario, *Adv. Funct. Mater.* **2017**, *27*, 1604740; b) C. Adda, B. Corraze, P. Stoliar, P. Diener, J. Tranchant, A. Filatre-Furcate, M. Fourmigué, D. Lorcy, M.-P. Besland, E. Janod, *J. Appl. Phys.* **2018**, *124*, 152124.

[43] a) J. H. Yoon, Z. Wang, K. M. Kim, H. Wu, V. Ravichandran, Q. Xia, C. S. Hwang, J. J. Yang, *Nat. Commun.* **2018**, *9*, 417; b) Z. Wang, M. Rao, J.-W. Han, J. Zhang, P. Lin, Y. Li, C. Li, W. Song, S. Asapu, R. Midya, *Nat. Commun.* **2018**, *9*, 3208.

[44] a) G. Palma, M. Suri, D. Querlioz, E. Vianello, B. De Salvo, presented at 2013 IEEE/ACM Int. Symp. on Nanoscale Architectures (NANOARCH), New York, NY, USA, July **2013**; b) X. Zheng, X. Li, J. Tang, B. Gao, H. Qian, H. Wu, presented at 2021 5th IEEE Electron Devices Technology & Manufacturing Conf. (EDTM), Chengdu, China, April **2021**.

[45] T. Danz, T. Domröse, C. Ropers, *Science* **2021**, *371*, 371.

[46] J. Cai, B. Fang, L. Zhang, W. Lv, B. Zhang, T. Zhou, G. Finocchio, Z. Zeng, *Phys. Rev. Appl.* **2019**, *11*, 034015.

[47] a) A. Sengupta, G. Srinivasan, D. Roy, K. Roy, presented at 2018 IEEE Int. Electron Devices Meeting (IEDM), San Francisco, CA, USA, December **2018**; b) Z.-x. Li, X.-y. Geng, J. Wang, F. Zhuge, *Front. Neurosci.* **2021**, *15*, 997; c) A. Mizrahi, T. Hirtzlin, A. Fukushima, H. Kubota, S. Yuasa, J. Grollier, D. Querlioz, *Nat. Commun.* **2018**, *9*, 1533.

© 2023 The Authors. Advanced Materials published by Wiley-VCH GmbH

15214095, 0, Downloaded from https://onlinelibrary.wiley.com/doi/10.1002/adma.202205047, Wiley Online Library on [19/06/2023]. See the Terms and Conditions (https://onlinelibrary.wiley.com/terms-and-conditions) on Wiley Online Library for rules of use; OA articles are governed by the applicable Creative Commons License

[48] a) A. Z. Pervaiz, L. A. Ghantasala, K. Y. Camsari, S. Datta, *Sci. Rep.* **2017**, *7*, 10994; b) V. Ostwal, P. Debashis, R. Faria, Z. Chen, J. Appenzeller, *Sci. Rep.* **2018**, *8*, 16689.
[49] S. Dutta, C. Schafer, J. Gomez, K. Ni, S. Joshi, S. Datta, *Front. Neurosci.* **2020**, *14*, 634.
[50] a) N. Shukla, S. Datta, A. Parihar, A. Raychowdhury, in *Future Trends in Microelectronics: Journey into the Unknown*, Wiley, New York **2016**, pp. 147–156; b) E. Vassilieva, G. Pinto, J. A. De Barros, P. Suppes, *IEEE Trans. Neural Networks* **2010**, *22*, 84.
[51] G. Csaba, W. Porod, *Appl. Phys. Rev.* **2020**, *7*, 011302.
[52] G. Csaba, A. Raychowdhury, S. Datta, W. Porod, presented at 2018 IEEE Int. Symp. on Circuits and Systems (ISCAS), Florence, Italy, May **2018**.
[53] a) T. C. Jackson, A. A. Sharma, J. A. Bain, J. A. Weldon, L. Pileggi, presented at 2015 IEEE 6th Latin American Symp. on Circuits & Systems (LASCAS), Montevideo, Uruguay, February **2015**; b) A. A. Sharma, J. A. Bain, J. A. Weldon, *IEEE J. Explor. Solid-State Comput. Devices Circuits* **2015**, *1*, 58.
[54] a) A. Raychowdhury, A. Parihar, G. H. Smith, V. Narayanan, G. Csaba, M. Jerry, W. Porod, S. Datta, *Proc. IEEE* **2018**, *107*, 73; b) A. Velichko, M. Belyaev, V. Putrolaynen, A. Pergament, V. Perminov, *Int. J. Mod. Phys. B* **2017**, *31*, 1650261; c) E. Corti, A. Khanna, K. Niang, J. Robertson, K. E. Moselund, B. Gotsmann, S. Datta, S. Karg, *IEEE Electron Device Lett.* **2020**, *41*, 629; d) J. Lin, S. Guha, S. Ramanathan, *Front. Neurosci.* **2018**, *12*, 856.
[55] a) K. Yogendra, D. Fan, K. Roy, *IEEE Trans. Magn.* **2015**, *51*, 4003909; b) M. Romera, P. Talatchian, S. Tsunegi, K. Yakushiji, A. Fukushima, H. Kubota, S. Yuasa, V. Cros, P. Bortolotti, M. Ernoult, *Nat. Commun.* **2022**, *13*, 883.
[56] E. Yu, A. Agrawal, D. Zheng, M. Si, M. Koo, D. Y. Peide, S. K. Gupta, K. Roy, *IEEE Electron Device Lett.* **2021**, *42*, 1670.
[57] a) C. Du, F. Cai, M. A. Zidan, W. Ma, S. H. Lee, W. D. Lu, *Nat. Commun.* **2017**, *8*, 2204; b) J. Moon, W. Ma, J. H. Shin, F. Cai, C. Du, S. H. Lee, W. D. Lu, *Nat. Electron.* **2019**, *2*, 480.
[58] M. Romera, P. Talatchian, S. Tsunegi, F. A. Araujo, V. Cros, P. Bortolotti, J. Trastoy, K. Yakushiji, A. Fukushima, H. Kubota, *Nature* **2018**, *563*, 230.
[59] M. Koo, M. Pufall, Y. Shim, A. B. Kos, G. Csaba, W. Porod, W. Rippard, K. Roy, *Phys. Rev. Appl.* **2020**, *14*, 034001.
[60] N. Shukla, W.-Y. Tsai, M. Jerry, M. Barth, V. Narayanan, S. Datta, presented at 2016 IEEE Symp. on VLSI Technology, Honolulu, HI, USA, June **2016**.
[61] G. F. Newell, E. W. Montroll, *Rev. Modern Phys.* **1953**, *25*, 353.
[62] a) W. Gerstner, W. M. Kistler, *Spiking Neuron Models: Single Neurons, Populations, Plasticity*, Cambridge University Press, Cambridge **2002**; b) A. N. Burkitt, *Biol. Cybern.* **2006**, *95*, 97.
[63] L. F. Abbott, *Brain Res. Bull.* **1999**, *50*, 303.
[64] a) D. Lee, M. Kwak, K. Moon, W. Choi, J. Park, J. Yoo, J. Song, S. Lim, C. Sung, W. Banerjee, *Adv. Electron. Mater.* **2019**, *5*, 1800866; b) H. Lim, H.-W. Ahn, V. Kornijcuk, G. Kim, J. Y. Seok, I. Kim, C. S. Hwang, D. S. Jeong, *Nanoscale* **2016**, *8*, 9629; c) S. Jia, H. Li, T. Gotoh, C. Longeaud, B. Zhang, J. Lyu, S. Lv, M. Zhu, Z. Song, Q. Liu, *Nat. Commun.* **2020**, *11*, 4636.
[65] a) Y.-F. Lu, Y. Li, H. Li, T.-Q. Wan, X. Huang, Y.-H. He, X. Miao, *IEEE Electron Device Lett.* **2020**, *41*, 1245; b) K. Wang, Q. Hu, B. Gao, Q. Lin, F.-W. Zhuge, D.-Y. Zhang, L. Wang, Y.-H. He, R. H. Scheicher, H. Tong, *Mater. Horiz.* **2021**, *8*, 619; c) X. Zhang, W. Wang, Q. Liu, X. Zhao, J. Wei, R. Cao, Z. Yao, X. Zhu, F. Zhang, H. Lv, *IEEE Electron Device Lett.* **2017**, *39*, 308; d) Y. Zhang, W. He, Y. Wu, K. Huang, Y. Shen, J. Su, Y. Wang, Z. Zhang, X. Ji, G. Li, *Small* **2018**, *14*, 1802188; e) L. Yan, Y. Pei, J. Wang, H. He, Y. Zhao, X. Li, Y. Wei, X. Yan, *Appl. Phys. Lett.* **2021**, *119*, 153507.
[66] a) H. Kalita, A. Krishnaprasad, N. Choudhary, S. Das, H.-S. Chung, Y. Jung, T. Roy, presented at 2018 76th Device Research Conf. (DRC), Santa Barbara, CA, USA, June **2018**; b) H. Kalita, A. Krishnaprasad, N. Choudhary, S. Das, D. Dev, Y. Ding, L. Tetard, H.-S. Chung, Y. Jung, T. Roy, *Sci. Rep.* **2019**, *9*, 53; c) L. Bao, J. Zhu, Z. Yu, R. Jia, Q. Cai, Z. Wang, L. Xu, Y. Wu, Y. Yang, Y. Cai, *ACS Appl. Mater. Interfaces* **2019**, *11*, 41482; d) D. Dev, A. Krishnaprasad, M. S. Shawkat, Z. He, S. Das, D. Fan, H.-S. Chung, Y. Jung, T. Roy, *IEEE Electron Device Lett.* **2020**, *41*, 936; e) C. J. Wan, L. Q. Zhu, Y. H. Liu, P. Feng, Z. P. Liu, H. L. Cao, P. Xiao, Y. Shi, Q. Wan, *Adv. Mater.* **2016**, *28*, 3557; f) D. Dev, M. S. Shawkat, A. Krishnaprasad, Y. Jung, T. Roy, *IEEE Electron Device Lett.* **2020**, *41*, 1440.
[67] a) D. W. Kim, W. S. Yi, J. Y. Choi, K. Ashiba, J. U. Baek, H. S. Jun, J. J. Kim, J. G. Park, *Front. Neurosci.* **2020**, *14*, 309; b) A. Jaiswal, S. Roy, G. Srinivasan, K. Roy, *IEEE Trans. Electron Devices* **2017**, *64*, 1818.
[68] a) S. Lashkare, S. Chouhan, T. Chavan, A. Bhat, P. Kumbhare, U. Ganguly, *IEEE Electron Device Lett.* **2018**, *39*, 484; b) J. Woo, D. Lee, Y. Koo, H. Hwang, *Microelectron. Eng.* **2017**, *182*, 42.
[69] a) Y. Chen, Y. Wang, Y. Luo, X. Liu, Y. Wang, F. Gao, J. Xu, E. Hu, S. Samanta, X. Wan, *IEEE Electron Device Lett.* **2019**, *40*, 1686; b) S. Hao, X. Ji, S. Zhong, K. Y. Pang, K. G. Lim, T. C. Chong, R. Zhao, *Adv. Electron. Mater.* **2020**, *6*, 1901335; c) P. Bousoulas, M. Panagopoulou, N. Boukos, D. Tsoukalas, *J. Phys. D: Appl. Phys.* **2021**, *54*, 225303; d) Y. Xu, H. Wang, D. Ye, R. Yang, Y. Huang, X. Miao, *IEEE Electron Device Lett.* **2021**, *43*, 116; e) T. Fu, X. Liu, H. Gao, J. E. Ward, X. Liu, B. Yin, Z. Wang, Y. Zhuo, D. J. Walker, J. J. Yang, *Nat. Commun.* **2020**, *11*, 1861; f) B. Dang, K. Liu, J. Zhu, L. Xu, T. Zhang, C. Cheng, H. Wang, Y. Yang, Y. Hao, R. Huang, *APL Mater.* **2019**, *7*, 071114.
[70] a) T. Roy, M. Tosun, X. Cao, H. Fang, D.-H. Lien, P. Zhao, Y.-Z. Chen, Y.-L. Chueh, J. Guo, A. Javey, ACS Nano **2015**, *9*, 2071; b) S. Kim, D. G. Roe, Y. Y. Choi, H. Woo, J. Park, J. I. Lee, Y. Choi, S. B. Jo, M. S. Kang, Y. J. Song, *Sci. Adv.* **2021**, *7*, eabe3996; c) J. Guo, Y. Liu, F. Zhou, F. Li, Y. Li, F. Huang, *Adv. Funct. Mater.* **2021**, *31*, 2102015.
[71] T. Kim, S. H. Kim, J. H. Park, J. Park, E. Park, S. G. Kim, H. Y. Yu, *Adv. Electron. Mater.* **2021**, *7*, 2000410.
[72] A. Kurenkov, S. DuttaGupta, C. Zhang, S. Fukami, Y. Horio, H. Ohno, *Adv. Mater.* **2019**, *31*, 1900636.
[73] a) S. Liu, C. H. Bennett, J. S. Friedman, M. J. Marinella, D. Paydarfar, J. A. C. Incorvia, *IEEE Magn. Lett.* **2021**, *12*, 4500805; b) W. H. Brigner, X. Hu, N. Hassan, C. H. Bennett, J. A. C. Incorvia, F. Garcia-Sanchez, J. S. Friedman, *IEEE J. Explor. Solid-State Comput. Devices Circuits* **2019**, *5*, 19; c) W. H. Brigner, N. Hassan, L. Jiang-Wei, X. Hu, D. Saha, C. H. Bennett, M. J. Marinella, J. A. C. Incorvia, F. Garcia-Sanchez, J. S. Friedman, *IEEE Trans. Electron Devices* **2019**, *66*, 4970.
[74] a) J. D. Valle, P. Salev, Y. Kalcheim, I. K. Schuller, *Sci. Rep.* **2020**, *10*, 4292; b) S. Oh, Y. Shi, J. D. Valle, P. Salev, Y. Lu, Z. Huang, Y. Kalcheim, I. K. Schuller, D. Kuzum, *Nat. Nanotechnol.* **2021**, *16*, 680.
[75] J. Wang, C. Teng, Z. Zhang, W. Chen, J. Tan, Y. Pan, R. Zhang, H. Zhou, B. Ding, H.-M. Cheng, *ACS Nano* **2021**, *15*, 15123.
[76] D. H. Perkel, G. L. Gerstein, G. P. Moore, *Biophys. J.* **1967**, *7*, 391.
[77] W. J. Ma, J. M. Beck, P. E. Latham, A. Pouget, Nat. Neurosci. **2006**, *9*, 1432.
[78] A. Dodda, S. J. A. n. Das, *ACS Nano* **2021**, *15*, 16172.
[79] a) D. C. Knill, A. Pouget, *Trends Neurosci.* **2004**, *27*, 712; b) L. Aitchison, M. Lengyel, *Curr. Opin. Neurobiol.* **2017**, *46*, 219.
[80] D. W. Kim, D. S. Woo, H. J. Kim, S. M. Jin, S. M. Jung, D. E. Kim, J. J. Kim, T. H. Shim, J. G. Park, *Adv. Electron. Mater.* **2022**, *8*, 2101356.
[81] B. Hille, *Biophys. J.* **1978**, *22*, 283.
[82] a) A. L. Hodgkin, A. F. Huxley, *J. Physiol.* **1952**, *117*, 500; b) J. Cronin, J. C. Boutelle, *Mathematical Aspects of Hodgkin–Huxley Neural Theory*, Cambridge University Press, Cambridge **1987**.
[83] L. Chua, *Nanotechnology* **2013**, *24*, 383001.

© 2023 The Authors. Advanced Materials published by Wiley-VCH GmbH

15214095, 0, Downloaded from https://onlinelibrary.wiley.com/doi/10.1002/adma.202205047, Wiley Online Library on [19/06/2023]. See the Terms and Conditions (https://onlinelibrary.wiley.com/terms-and-conditions) on Wiley Online Library for rules of use; OA articles are governed by the applicable Creative Commons License

[84] W. Yi, K. K. Tsang, S. K. Lam, X. Bai, J. A. Crowell, E. A. Flores, *Nat. Commun.* **2018**, *9*, 4661.
[85] Q. Ma, M. R. Haider, V. L. Shrestha, Y. Massoud, *Analog Integr. Circuits Signal Process.* **2012**, *73*, 329.
[86] a) A. Moujahid, A. d'Anjou, F. Torrealdea, F. Torrealdea, *Phys. Rev. E* **2011**, *83*, 031912; b) Y. Wang, R. Wang, X. Xu, *Neural Plast.* **2017**, *2017*, 6207141; c) F. Zhu, R. Wang, X. Pan, Z. Zhu, *Cognit. Neurodyn.* **2019**, *13*, 75; d) A. Payeur, J. Guerguiev, F. Zenke, B. A. Richards, R. Naud, *Nat. Neurosci.* **2021**, *24*, 1010.
[87] H. M. Huang, R. Yang, Z. H. Tan, H. K. He, W. Zhou, J. Xiong, X. Guo, *Adv. Mater.* **2019**, *31*, 1803849.
[88] M. D. Pickett, R. S. Williams, *Nanotechnology* **2013**, *24*, 384002.
[89] S. Kumar, R. S. Williams, Z. Wang, *Nature* **2020**, *585*, 518.
[90] a) V. E. Abraira, D. D. Ginty, *Neuron* **2013**, *79*, 618; b) E. A. Lumpkin, M. J. Caterina, *Nature* **2007**, *445*, 858.
[91] M. A. Zidan, J. P. Strachan, W. D. Lu, *Nat. Electron.* **2018**, *1*, 22.
[92] a) W. Chen, Z. Zhang, G. Liu, *iScience* **2022**, *25*, 103729; b) W. Pan, J. Zheng, L. Wang, Y. Luo, *Engineering* **2022**, *14*, 19.
[93] a) F. Zhou, Y. Chai, *Nat. Electron.* **2020**, *3*, 664; b) M. Wang, Y. Luo, T. Wang, C. Wan, L. Pan, S. Pan, K. He, A. Neo, X. Chen, *Adv. Mater.* **2021**, *33*, 2003014.
[94] a) F. Zhou, Z. Zhou, J. Chen, T. H. Choy, J. Wang, N. Zhang, Z. Lin, S. Yu, J. Kang, H. P. Wong, Y. Chai, *Nat. Nanotechnol.* **2019**, *14*, 776; b) C.-Y. Wang, S.-J. Liang, S. Wang, P. Wang, Z. a. Li, Z. Wang, A. Gao, C. Pan, C. Liu, J. Liu, H. Yang, X. Liu, W. Song, C. Wang, B. Cheng, X. Wang, K. Chen, Z. Wang, K. Watanabe, T. Taniguchi, J. J. Yang, F. Miao, *Sci. Adv.* **2020**, *6*, eaba6173; c) Y. Lee, J. Y. Oh, W. Xu, O. Kim, T. R. Kim, J. Kang, Y. Kim, D. Son, J. B.-H. Tok, M. J. Park, Z. Bao, T.-W. Lee, *Sci. Adv.* **2018**, *4*, eaat7387; d) S. Seo, S. H. Jo, S. Kim, J. Shim, S. Oh, J. H. Kim, K. Heo, J. W. Choi, C. Choi, S. Oh, D. Kuzum, H. P. Wong, J. H. Park, *Nat. Commun.* **2018**, *9*, 5106.
[95] L. Bao, J. Kang, Y. Fang, Z. Yu, Z. Wang, Y. Yang, Y. Cai, R. Huang, *Sci. Rep.* **2018**, *8*, 13727.
[96] Q. Wu, B. Dang, C. Lu, G. Xu, G. Yang, J. Wang, X. Chuai, N. Lu, D. Geng, H. Wang, L. Li, *Nano Lett.* **2020**, *20*, 8015.
[97] B. Mu, L. Guo, J. Liao, P. Xie, G. Ding, Z. Lv, Y. Zhou, S. T. Han, Y. Yan, *Small* **2021**, *17*, 2103837.
[98] C. Chen, Y. He, H. Mao, L. Zhu, X. Wang, Y. Zhu, Y. Zhu, Y. Shi, C. Wan, Q. Wan, *Adv. Mater.* **2022**, *34*, 2201895.
[99] J. K. Han, D. M. Geum, M. W. Lee, J. M. Yu, S. K. Kim, S. Kim, Y. K. Choi, *Nano Lett.* **2020**, *20*, 8781.
[100] J.-K. Han, J. Sim, D.-M. Geum, S. K. Kim, J.-M. Yu, J. Kim, S. Kim, Y.-K. Choi, presented at *2021 IEEE Int. Electron Devices Meeting (IEDM)*, San Francisco, CA, USA, December **2021**.
[101] L. Mennel, J. Symonowicz, S. Wachter, D. K. Polyushkin, A. J. Molina-Mendoza, T. Mueller, *Nature* **2020**, *579*, 62.
[102] Z. Zhang, S. Wang, C. Liu, R. Xie, W. Hu, P. Zhou, *Nat. Nanotechnol.* **2022**, *17*, 27.
[103] S. Lee, R. Peng, C. Wu, M. Li, *Nat. Commun.* **2022**, *13*, 1485.
[104] A. Zimmerman, L. Bai, D. D. Ginty1, J. Y. Oh, *Science* **2014**, *346*, 950.
[105] B. Zhu, H. Wang, Y. Liu, D. Qi, Z. Liu, H. Wang, J. Yu, M. Sherburne, Z. Wang, X. Chen, *Adv. Mater.* **2016**, *28*, 1559.
[106] a) Y. Zang, H. Shen, D. Huang, C. A. Di, D. Zhu, *Adv. Mater.* **2017**, *29*, 1606088; b) Q. Xia, Y. Qin, A. Zheng, P. Qiu, X. Zhang, *Adv. Mater. Interfaces* **2021**, *8*, 2101068.
[107] C. Zhang, W. B. Ye, K. Zhou, H. Y. Chen, J. Q. Yang, G. Ding, X. Chen, Y. Zhou, L. Zhou, F. Li, S. T. Han, *Adv. Funct. Mater.* **2019**, *29*, 1808783.
[108] C. Wan, G. Chen, Y. Fu, M. Wang, N. Matsuhisa, S. Pan, L. Pan, H. Yang, Q. Wan, L. Zhu, X. Chen, *Adv. Mater.* **2018**, *30*, 1801291.
[109] S. Kim, Y. Lee, H.-D. Kim, S.-J. Choi, *NPG Asia Mater.* **2020**, *12*, 76.
[110] F. Yu, J. C. Cai, L. Q. Zhu, M. Sheikhi, Y. H. Zeng, W. Guo, Z. Y. Ren, H. Xiao, J. C. Ye, C. H. Lin, A. B. Wong, T. Wu, *ACS Appl. Mater. Interfaces* **2020**, *12*, 26258.
[111] J. Zhu, X. Zhang, M. Wang, R. Wang, P. Chen, L. Cheng, Q. Liu, *IEEE Electron Device Lett.* **2022**, *43*, 962.
[112] a) Y. Kim, A. Chortos, W. Xu, Y. Liu, J. Y. Oh, D. Son, J. Kang, A. M. Foudeh, C. Zhu, Y. Lee, *Science* **2018**, *360*, 998; b) H. Tan, Q. Tao, I. Pande, S. Majumdar, F. Liu, Y. Zhou, P. O. Persson, J. Rosen, S. van Dijken, *Nat. Commun.* **2020**, *11*, 1369.
[113] C. Wan, P. Cai, X. Guo, M. Wang, N. Matsuhisa, L. Yang, Z. Lv, Y. Luo, X. J. Loh, X. Chen, *Nat. Commun.* **2020**, *11*, 4602.
[114] Q. Duan, T. Zhang, C. Liu, R. Yuan, G. Li, P. J. Tiw, K. Yang, C. Ge, Y. Yang, R. Huang, *Adv. Intell. Syst.* **2022**, *4*, 2200039.
[115] R. Yuan, Q. Duan, P. J. Tiw, G. Li, Z. Xiao, Z. Jing, K. Yang, C. Liu, C. Ge, R. Huang, *Nat. Commun.* **2022**, *13*, 3973.
[116] J. Zhu, X. Zhang, R. Wang, M. Wang, P. Chen, L. Cheng, Z. Wu, Y. Wang, Q. Liu, M. Liu, *Adv. Mater.* **2022**, *34*, 2200481.
[117] J.-K. Han, S.-C. Park, J.-M. Yu, J.-H. Ahn, Y.-K. Choi, *Nano Lett.* **2022**, *22*, 5244.
[118] S. B. Laughlin, R. R. de Ruyter van Steveninck, J. C. Anderson, *Nat. Neurosci.* **1998**, *1*, 36.
[119] M. S. Mian, K. Okimura, J. Sakai, *J. Appl. Phys.* **2015**, *117*, 215305.
[120] Y. Kalcheim, A. Camjayi, J. D. Valle, P. Salev, M. Rozenberg, I. K. Schuller, *Nat. Commun.* **2020**, *11*, 2985.
[121] a) A. Mellnik, J. Lee, A. Richardella, J. Grab, P. Mintun, M. H. Fischer, A. Vaezi, A. Manchon, E.-A. Kim, N. Samarth, *Nature* **2014**, *511*, 449; b) Q. Zhang, K. Chan, J. Li, *Sci. Rep.* **2018**, *8*, 4343.
[122] H. Zhao, Z. Dong, H. Tian, D. DiMarzi, M. G. Han, L. Zhang, X. Yan, F. Liu, L. Shen, S. J. Han, S. Cronin, W. Wu, J. Tice, J. Guo, H. Wang, *Adv. Mater.* **2017**, *29*, 1703232.
[123] S. Raoux, *Annu. Rev. Mater. Res.* **2009**, *39*, 25.
[124] a) A. A. Bessonov, M. N. Kirikova, D. I. Petukhov, M. Allen, T. Ryhänen, M. J. Bailey, *Nat. Mater.* **2015**, *14*, 199; b) D. Son, S. I. Chae, M. Kim, M. K. Choi, J. Yang, K. Park, V. S. Kale, J. H. Koo, C. Choi, M. Lee, *Adv. Mater.* **2016**, *28*, 9326.
[125] Y. He, P. Tang, Z. Hu, Q. He, C. Zhu, L. Wang, Q. Zeng, P. Golani, G. Gao, W. Fu, *Nat. Commun.* **2020**, *11*, 57.
[126] R. Patel, E. Ipek, E. Friedman, presented at 2012 IEEE Int. SOC Conf., New York, NY, USA, September **2012**.
[127] R. Wigington, *Proc. IRE* **1959**, *47*, 516.
[128] F. C. Hoppensteadt, E. M. Izhikevich, *Phys. Rev. Lett.* **1999**, *82*, 2983.
[129] R. Follmann, E. E. Macau, E. Rosa, J. R. Piqueira, *IEEE Trans. Neural Networks Learn. Syst.* **2014**, *26*, 1539.
[130] B. Popescu, G. Csaba, D. Popescu, A. H. Fallahpour, P. Lugli, W. Porod, M. Becherer, *J. Appl. Phys.* **2018**, *124*, 152128.
[131] A. Todri-Sanial, S. Carapezzi, C. Delacour, M. Abernot, T. Gil, E. Corti, S. F. Karg, J. Nüñez, M. Jiménèz, M. J. Avedillo, *IEEE Trans. Neural Networks Learn. Syst.* **2021**, *33*, 1996.
[132] H. Paugam-Moisy, S. M. Bohte, in *Handbook of Natural Computing* (Eds: G. Rozenberg, T. Bäck, J. N. Kok), Springer, New York **2012**, pp. 335–376.
[133] S. Yang, J. Shin, T. Kim, K.-W. Moon, J. Kim, G. Jang, D. S. Hyeon, J. Yang, C. Hwang, Y. Jeong, *NPG Asia Mater.* **2021**, *13*, 11.
[134] S. M. Bohte, J. N. Kok, H. L. Poutre, *Neurocomputing* **2002**, *48*, 17.
[135] S. McKennoch, T. Voegtlin, L. Bushnell, *Neural Comput.* **2009**, *21*, 9.
[136] D. Huh, T. J. Sejnowski, presented at *Advances in Neural Information Processing Systems*, Montréal, Canada, December **2018**.
[137] F. Zenke, S. Ganguli, *Neural Comput.* **2018**, *30*, 1514.
[138] T. P. Lillicrap, A. Santoro, L. Marris, C. J. Akerman, G. Hinton, *Nat. Rev. Neurosci.* **2020**, *21*, 335.
[139] W. Gerstner, J. van Hemmen, presented at *Advances in Neural Information Processing Systems*, Denver, CO, USA, December **1993**.
[140] G. Zhang, D. Guo, F. Wu, J. Ma, *Neurocomputing* **2020**, *379*, 296.

© 2023 The Authors. Advanced Materials published by Wiley-VCH GmbH

15214095, 0, Downloaded from https://onlinelibrary.wiley.com/doi/10.1002/adma.202205047, Wiley Online Library on [19/06/2023]. See the Terms and Conditions (https://onlinelibrary.wiley.com/terms-and-conditions) on Wiley Online Library for rules of use; OA articles are governed by the applicable Creative Commons License

[141] M. Ignatov, M. Ziegler, M. Hansen, H. Kohlstedt, *Sci. Adv.* **2017**, *3*, e1700849.
[142] W. Wang, G. Pedretti, V. Milo, R. Carboni, A. Calderoni, N. Ramaswamy, A. S. Spinelli, D. Ielmini, *Sci. Adv.* **2018**, *4*, eaat4752.
[143] J. J. Hopfield, C. D. Brody, *Proc. Natl. Acad. Sci. U. S. A.* **2001**, *98*, 1282.
[144] a) A. Serb, J. Bill, A. Khiat, R. Berdan, R. Legenstein, T. Prodromakis, *Nat. Commun.* **2016**, *7*, 12611; b) S. Yu, B. Gao, Z. Fang, H. Yu, J. Kang, H. S. P. Wong, *Adv. Mater.* **2013**, *25*, 1774; c) T. Tuma, M. L. Gallo, A. Sebastian, E. Eleftheriou, *IEEE Electron Device Lett.* **2016**, *37*, 1238; d) A. Sebastian, T. Tuma, N. Papandreou, M. L. Gallo, L. Kull, T. Parnell, E. Eleftheriou, *Nat. Commun.* **2017**, *8*, 1115.
[145] J.-K. Han, M. Seo, W.-K. Kim, M.-S. Kim, S.-Y. Kim, M.-S. Kim, G.-J. Yun, G.-B. Lee, J.-M. Yu, Y.-K. Choi, *IEEE Electron Device Lett.* **2019**, *41*, 208.
[146] a) E. T. Vu, F. B. Krasne, *Science* **1992**, *255*, 1710; b) J. Snoek, R. Zemel, R. P. Adams, presented at Advances in Neural Information Processing Systems, Lake Tahoe, NV, USA, December **2013**.
[147] a) H. Zeng, J. R. Sanes, *Nat. Rev. Neurosci.* **2017**, *18*, 530; b) U. Hasson, S. A. Nastase, A. Goldstein, *Neuron* **2020**, *105*, 416.
[148] a) J. E. Ledoux, D. A. Ruggiero, R. Forest, R. Stornetta, D. J. Reis, *J. Comp. Neurol.* **1987**, *264*, 123; b) C. Van Eden, J. Kros, H. Uylings, *Prog. Brain Res.* **1991**, *85*, 169.
[149] T. Matsui, M. Amagai, *Int. Immunol.* **2015**, *27*, 269.
[150] T. Someya, M. Amagai, *Nat. Biotechnol.* **2019**, *37*, 382.
[151] a) M. Kaltenbrunner, T. Sekitani, J. Reeder, T. Yokota, K. Kuribara, T. Tokuhara, M. Drack, R. Schwödiauer, I. Graz, S. Bauer-Gogonea, *Nature* **2013**, *499*, 458; b) Y. van De Burgt, A. Melianas, S. T. Keene, G. Malliaras, A. Salleo, *Nat. Electron.* **2018**, *1*, 386.
[152] a) A. Longtin, *J. Stat. Phys.* **1993**, *70*, 309; b) S.-G. Lee, A. Neiman, S. Kim, *Phys. Rev. E* **1998**, *57*, 3292; c) Y. Yu, W. Wang, J. Wang, F. Liu, *Phys. Rev. E* **2001**, *63*, 021907.
[153] L. Buesing, J. Bill, B. Nessler, W. Maass, *PLoS Comput. Biol.* **2011**, *7*, e1002211.

Hefei Liu is currently a Ph.D. candidate in the Ming Hsieh Department of Electrical and Computer Engineering at University of Southern California. He received his B.S. in physics from Peking University. His research interests include neuromorphic computing and nanoelectronics based on vdW materials.

Yuan Qin is currently a postdoctoral associate at Center for Power Electronics Systems, Virginia Tech. He obtained his Ph.D. in microelectronics and solid electronics from Institute of Microelectronics, Chinese Academy of Sciences in 2021. His research interests focus on wide-bandgap semiconductor devices toward applications for deep UV photonics and power electronics.

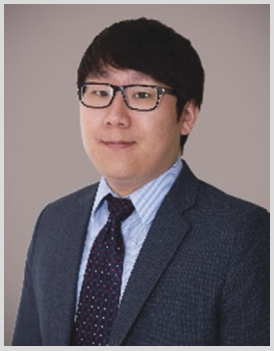

Yuhao Zhang received the B.S. degree from Peking University, Beijing, China, in 2011, and the M.S. and Ph.D. degrees from Massachusetts Institute of Technology (MIT), Cambridge, MA, USA, in 2013 and 2017, respectively. From 2017 to 2018, he was a postdoctoral associate with MIT. Since 2018, he has been an assistant professor with the Center for Power Electronics Systems, Virginia Tech. His research interests include emerging semiconductor devices, (ultra-)wide-bandgap semiconductor materials, power electronics, and machine learning assisted co-design. He has published over 100 journal articles and conference proceedings and is an inventor of five granted U.S. patents.

© 2023 The Authors. Advanced Materials published by Wiley-VCH GmbH

15214095, 0, Downloaded from https://onlinelibrary.wiley.com/doi/10.1002/adma.202205047, Wiley Online Library on [19/06/2023]. See the Terms and Conditions (https://onlinelibrary.wiley.com/terms-and-conditions) on Wiley Online Library for rules of use; OA articles are governed by the applicable Creative Commons License

Han Wang is currently an associate professor of electrical and computer engineering and holder of the Robert G. and Mary G. Lane Early Career Chair at University of Southern California, which he joined since 2014. In 2021–2023, he also led the low dimensional materials research at Taiwan Semiconductor Manufacturing Company (TSMC) Corporate Research while on leave from USC. He received his B.A. degree in electrical and information science from Cambridge University in 2007 and his Ph.D. degree from Massachusetts Institute of Technology in 2013. From 2013 to 2014, he worked at IBM T.J. Watson Research Center. His research interests include the fundamental study and device innovation in electronics and photonics technology based on emerging nanomaterials for computing, communication, and sensing applications.

© 2023 The Authors. Advanced Materials published by Wiley-VCH GmbH

15214095, 0, Downloaded from https://onlinelibrary.wiley.com/doi/10.1002/adma.202205047, Wiley Online Library on [19/06/2023]. See the Terms and Conditions (https://onlinelibrary.wiley.com/terms-and-conditions) on Wiley Online Library for rules of use; OA articles are governed by the applicable Creative Commons License